Jour. Fac. Sci., Hokkaido Univ., Ser. VII (Geophysics), Vol. 7, No. 4, 339-399, 1984.

The Effect of Cracks on Compressional Wave Velocity and Its Anisotropy in Calcareous Rocks

Nobuyuki Shimizu

Department of Geophysics, Faculty of Science, Hokkaido University, Sapporo 060, Japan

(Received October 29, 1983)

Abstract

The compressional wave velocity (Vp) and the strain were measured as a function of confining pressure (Pc) for two kinds of low porosity rock, fine and coarse grained rocks. The samples used are composed of the carbonate minerals. The measurements showed that the Vp increase by confining pressure is due to the closing of pre-existing cracks in a rock. Based on the relation between the measured Vp and confining pressure, distributions of shapes of pre-existing cracks in rocks were calculated inversely and were exhibited by the crack porosity for a given aspect ratio. For both rocks, the porosity distribution has a maximum in the range of aspect ratio 10^{-4}-10^{-3}. The porosities of cracks with aspect ratio larger than about 4×10^{-4}, and the total crack porosity for the fine grained rock are greater than those for the coarse grained rock. For both rocks, the different distributions of shapes of pre-existing cracks satisfactorily explain the differences in the $Vp-Pc$ relation and in the strain-Pc relation.

The change of Vp and its anisotropy (VA) due to confining pressure and differential stress was experimentally investigated for both rock samples. For the investigation of the VA, the compressional wave velocities were measured for three directions in the samples as a function of differential stress under five different confining pressures each of which was, however, kept at constant during a measurement. These measurements could display clear evidence of the VA for both rocks at every confining pressure. In the range of confining pressure measured, the VA was observed to consist of two phases. These phases seem to be closely related to the generation mechanism of the VA. The first phase is due to compaction by the closing of pre-existing cracks in rocks and the second phase is due to dilatancy which could generate new cracks in rocks one after another. The characteristics of the measured VA can be summarized as: (1) The Va (the extent of VA) of the first phase increases rapidly with increasing differential stress and reaches its maximum (Va^{max}) at a differential stress. The maximum value of VA, Va^{max}, decreases exponentially as confining pressure increases. (2) The Va of the second phase increases exponentially with increasing differential stress. In addition, the Va also increases rapidly with increasing volumetric strain in the first stage of dilatancy, and in the second stage of dilatancy, the increasing rate of the Va becomes lower than before.

During these measurements, a differential stress at which dilatancy begins (called onstet stress) was determined from a curve which smoothes the measured Va against differential stress. The onset stress thus determined agrees well with that determined

by the usual method from a stress-strain curve. Even when it is difficult to determine the onset stress of dilatancy from a stress-strain curve for uniaxial compression, our method could easily give the onset stress.

The experimental results on the anisotropic Vp changes and on the volumetric strain changes were investigated by using Eshelby's theory on the problem of inclusion. The theoretical investigation was made on the Vp and strain change as a function of confining pressure and differential stress using the distribution of shapes of pre-existing cracks. The measured Vp and strain under triaxial stress, except the measured Vp under uniaxial stress, could be explained by extending Eshelby's theory. It was confirmed that the effect of the crack interaction on Vp is not negligibly small. It was proved that the Va^{max} is linearly related to the increase of Vp at a differential stress of zero, and that the relation has a negative slope. From the characteristic Vp and strain changes for the physical process of dilatancy, it was inferred that the aspect ratios of dilatant cracks grow as dilatancy advances.

1. Introduction

It is well known that rocks exhibit an anisotropy in physical and mechanical properties. The anisotropy is generally caused by a preferred orientation of menerals composing a rock and differential stress (σ). The anisotropy due to differential stress was observed to appear in electrical resistivity (Fujii and Hamano, 1977), in attenuation of elastic wave energy (Lockner et al., 1977; Shimizu and Maeda, 1980) and in dilatancy (Hadley, 1975; Scholz and Koczynski, 1979).

Clear evidences of the anisotropy due to differential stress have also been found in elastic wave velocities. Tocher (1975) measured compressional wave velocities (Vp) of seven kinds of rocks in directions parallel to and perpendicular to a load axis under uniaxial compression, and showed that the anisotropy (VA) of compressional wave velocity is detected in most rocks. Nur and Simmons (1969 a) measured compressional and shear wave velocities of Barre granite in ten directions by the Brazilian test under atmospheric pressure. Their measurements show that the measured values of the compressional wave velocities are given as a function of $\cos 2\theta$, where θ is an angle between the direction of propagation and the load axis. In addition, they observed that two shear waves exhibit acoustic double refraction. This acoustic double refraction was also observed by Bonner (1974) for Westerly granite under uniaxial compression. Gupta (1973) measured compressional and shear wave velocities of Indiana limestone under uniaxial compression in three directions which correspond to the principal stress axes, respectively, and showed that the velocity anisotropy increases with increasing differential stress. Soga et al. (1978) measured compressional and shear wave velocities of Westerly granite as a

function of differential stress under confining pressures of 0.5 and 1.0 kbars in three directions which correspond to the principal stress axes, respectively, and estimated the shape of dilatant cracks using a penny-shaped crack model from anisotropic velocity changes.

Most studies on the anisotropy of elastic wave velocity, except for the study by Soga et al. (1978), have only given the speculation that the main cause of the anisotropy might be cracks in rocks. This speculation may be convinced because macroscopically isotropic rocks also often exhibit the anisotropy by the application of differential stress. To make the cause of the anisotropy clear qualitatively, it is necessary to know a physical relationship of the anisotropy to confining pressure, differential stress and volumetric strain. However, a clear relationship among those quantities has not been obtained yet, since the physical conditions and tested rocks were different in these experiments. If systematic experiments are carried out under the condition that a unified experimental apparatus is always used and rocks are carefully selected for the purpose, some definite relationship will be obtained.

The anisotropy to be revealed by the experiment is also applicable to a problem to determine accurate AE (acoustic emission) hypocenters; there is a good example that wrong determination of AE hypocenters was largely improved by taking the anisotropy of compressional wave velocity into account for the experiment made on a very large granite sample under uniaxial compression (Shimizu and Maeda, 1982).

If the cause of the anisotropy is cracks in rocks, it may be said that cracks or crack distributions in rocks have a key to solve the problem how the anisotropy is induced in rocks, as well as the problem how differential stress affects the physical and mechanical properties of rocks. A number of authors have proposed theories to quantitatively explain the physical and mechanical properties of a medium containing cracks. Brace et al. (1968) derived a theoretical relation between permeability and electrical resistivity on the basis of the interconnection of cracks, and showed that the relation agrees well with the experimental relation. Eshelby (1957) developed a method to solve the elastic field of an ellipsoidal inclusion and related problems. Walsh (1965 a) investigated the effect of elliptical cracks on the compressibility of rocks. Nur (1971) derived the expressions for the effective elastic wave velocities for an isotropic modium containing penny-shaped cracks. O'Connell and Budiansky (1974) calculated the effective elastic moduli of a medium permeated with an isotropic distribution of elliptical cracks from the energy of a single crack using a self-consistent method. Kuster and Toksöz (1974) calculated the effective

elastic moduli of a medium permeated with an isotropic distribution of ellipsoidal cracks on the basis of scattering theory. Mavko and Nur (1978) and Walsh and Grosenbaugh (1979) investigated the effect of nonelliptical cracks on the compressibility of rocks. Although it is desirable that the physical and mechanical properties of rocks can be explained quantitatively by a unified theory, it is very difficult to construct such a theory. There is no investigation in which the anisotropic Vp and strain changes as a function of stress are quantitatively analyzed simultaneously and systematically. Therefore, we will investigate whether the anisotropic Vp and strain changes due to differential stress, and the Vp and strain changes due to confining pressure can be explained quantitatively by a unified theory or not.

The purpose of the present study is to reveal the mechanism to induce the anisotropy of compressional wave velocity in rocks, for which systematic measurements of compressional wave velocities and strains will be made on specified rock species under some confining pressures. The characteristics of the anisotropic Vp change and the strain change will be described as a function of differential stress through the experiments and will be explained by the theory which is an extension of Eshelby's theory to the elastic field of a medium containing ellipsoidal cracks.

2. Experiments

2.1 Samples

Rock samples used in this study were selected by the following criterions: (1) rocks being almost entirely composed of one kind of mineral, (2) rocks having no preferred orientation of minerals, and (3) rocks being composed of grains with nearly equal dimention. Criterion (1) facilitates estimating crack-free elastic parameters of the rock samples without data on elastic wave velocities at a high confining pressure over 5 kbars. Criterion (2) facilitates to make the cause of the velocity anisotropy clear. Crinterion (3) is useful to investigate the effect of a grain size on the quantities to be measured.

According to the above criterions, the samples of two kinds of rocks, having a size of $5\times5\times15$ cm, were prepared; one is a coarse grained marble from Yamaguchi, Japan (which is abbreviated as CGM hereafter), and the other, a fine grained dolostone from Yugoslavia (which is abbrevated as FGM hereafter). The sides of the sample being opposite to each other were ground to be parallel to each other within an accuracy of ±0.005 cm. The physical parameters of these rocks are given in Table 1. The parameters were measured by the usual

Table 1 Physical parameters of rocks used in this study

	CGM	FGM
Mean grain size (mm)	2.5	0.3
Density (g/cc)	2,711±0.002	2.855±0.006
Porosity (%)	0.25±0.01	0.36±0.01
Vp(km/sec)	4.88±0.20	4.08±0.20
Vs (km/sec)	2.64±0.04	2.39±0.02
Tensile strength (bar)	16±3	34±5
Compressive strength (Kbar)	0.8±0.1	1.6±0.1
Bulk modulus (Mbar) K	0.75	1.048
Shear modulus (Mbar) G	0.346	0.311

The values of Vp and Vs are those measured at atmospheric pressure. The values of bulk and shear moduli are those for crack-free medium.

methods. The crack-free elastic moduli of the rocks, bulk modulus K and shear modulus G, were estimated from the physical constants given by Clark (1966) and Simmons and Wang (1971).

Before the experiments, these samples were dried in a desiccator at room temperature for more than a week. The compressional wave velocities of the samples were, within the limit of experimental error, equal to those of samples which were dried at 120℃ for an hour. Therefore the effect of water on Vp can be neglected through the experiments.

2.2 Experimental Apparatus

Figure 1 shows a cross section of the pressure vessel and some assemblies in the experimental apparatus of which a detailed explanation has previously been given by Maeda (1979). In this section, the method employed in this experiment for applying confining pressure and differential stress to the samples will briefly be described.

The apparatus is capable of making fracture experiments of rocks under confining pressures up to 2 kbars. For the experiment, the rock sample sealed by silicone resin is set between the upper and lower platens in the pressure vessel with a load cell which is used to measure a differential stress. The confining pressure can be applied to the sample by pouring oil into the pressure room and the differential stress by pressing down the inner piston built in the main piston

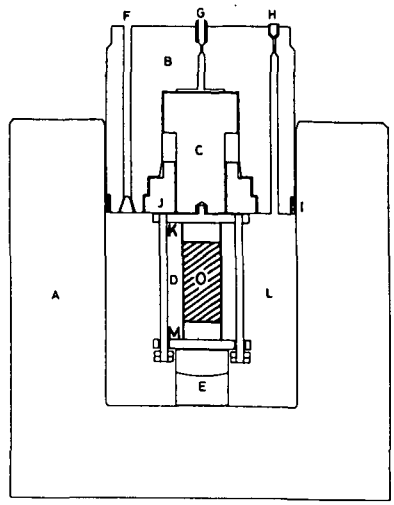

Fig. 1 Cross section of pressure vessel and some assemblies in the experimental apparatus (after Maeda, 1979). A: main cylinder, B: main piston, C: inner piston, D: lods for supporting M and sample, E: bowl base, F: holes for lead-wires, G: connector for axial pressure oil, H: air relief valve, I: oil seal, J: nut, K and M: platens, L: high pressure room, O: sample.

as shown in Fig. 1. The confining pressure and differential stress can be measured within the limit of ± 10 bars.

2.3 Measurements of Velocities and Strains

A block diagram of the measurement system is shown in Fig. 2 (b). Anisotropic properties of rocks may be confirmed by investigating an azimuthal dependency of velocities of the rocks. For the investigation, three sensors are placed on the sample surface as shown in Fig. 2 (a). These sensors are used to measure the velocities of compressional waves propagating from a transmitter placed on the opposite surface to these sensors with the directions of 10°, 45° and 90°. Both the sensors and the transmitter used, being piezoelectric transducers with a resonant frequency of 2 *MHz* in a compressional mode, are fixed on the rock surface by epoxy.

In the experiment, the compressional wave velocities for the three directions were measured under various confining pressures and also under various differential stresses while a confining pressure was being kept at constant. A method of the Vp measurement employed is the pulse transmission method developed by Birch (1960). Axial and lateral strains for the rock sample under the same confining pressures and differential stresses were simultaneously

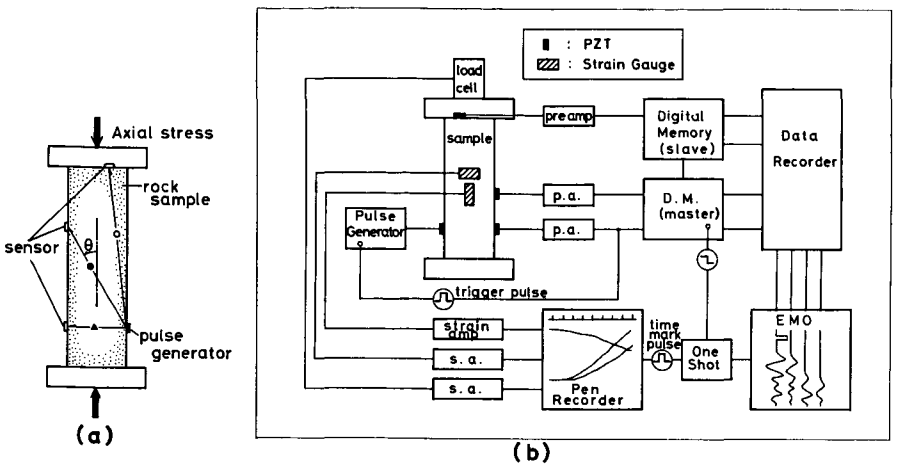

Fig. 2 Measurement system. (a) Arrangement of sensors and a transmitter for Vp measurement in three directions. (b) Block diagram of the measurement system for velocities and strains. Signals recieved by sensors are recorded by a data recorder, and strains by a pen recorder.

simultaneously measured also. Strain gauges used for the measurement being 1 cm long are fixed to the central part of the rock sample by epoxy.

For each rock sample, both velocities and strains were measured not only under various confining pressures while no differential stress being applied, but also under various differential stresses while a confining pressure was being kept at constant. The whole measurement scheme is listed in Table 2. The measurement procedure is as follows: first, while the confining pressure is raised from atmospheric pressure to a certain value with an electromotive pump, the velocity is measured (such a measurement is denoted by *HP* in Table 2); and second, while the confining pressure is being kept at that value, the velocity and strain are measured for different differential stresses (such a measurement is denoted by *DS* in Table 2). To apply the differential stress to the rock sample in the slow stress rate, the loading was made by a hand pump during all the experiments. The loading system was manually controlled during the experiments for CGM except for CGM-3, while it was automatically controlled during the experiments for FGM except for FGM-1. The mean stress rate was 0.9-2.3 bars/sec which corresponds to about 10^{-6}-2.5×10^{-6}/sec in strain rate. Table 2 shows the data acquisition on the velocities and on the strains. In some measurements, all data were not obtained. The accuracy of the measurement of velocities and strains were within ±0.05 km/sec and within $\pm3\times10^{-5}$, respectively.

Table 2 List of experiments and data acquisition

No.	experimental condition		Vp			strain	
			10°	45°	90°	axial	lateral
CGM-1	DS	Ph=1 bar	○	○	○	○	○
CGM-2	DS	Pc=200 bars	○	○	—	○	○
CGM-3	DS, HP	Pc=300 bars	○	○	○	○	○
CGM-4	DS	Pc=470 bars	○	○	○	○	—
CGM-5	DS	Pc=970 bars	○	△	△	○	○
CGM-6	HP		○	○	○	○	○
FGM-1	DS	Pc=1 bar	○	○	○	○	○
FGM-2	DS, HP	Pc=180 bars	○	○	○	○	○
FGM-3	DS	Pc=410 bars	○	○	○	○	○
FGM-4	DS, HP	Pc=570 bars	○	○	○	○	○
FGM-5	DS, HP	Pc=940 bars	○	○	○	○	○
FGM-6	HP		○	○	○	○	○

DS; experiment under differential stress
HP; experiment under hydrostatic pressure
Pc; hydrostatic confining pressure held at constant during an experiment
○; complete data set (all data was obtained.)
△; uncomplete data set (some data were not obtained.)
—; no data was obtained due to sensor trouble.

3. Experimental Results and Theoretical Considerations

3.1 Vp Change due to Confining Pressure

(i) Experimental Results

We measured compressional wave velocities and volumetric strains for two kinds of rocks at different confining pressures up to 1.5 kbars. Figure 4 shows the compressional wave velocities and the volumetric strains measured for CGM as a function of confining pressure and Fig. 5 those for FGM as a function of confining pressure. In these figures, the compressional wave velocities and volumetric strains calculated according to the procedure, which will be mentioned in section 3.1-(iii), are also shown; however, these will be discussed in detail in section 3.1-(iv).

The measured *Vp's* at the same confining pressure differ from sample to sample by 10% at most for CGM and by 7% at most for FGM. This means that analyzing the *Vp* data, we must take this amount of scatter into account. The amounts of the *Vp* increase with a confining pressure up to 1 kbars are about 30-

43% for CGM and 63-75% for FGM. The Vp change due to confining pressure for CGM is different from that for FGM. At confining pressures lower than a certain value (which we call a transitional pressure, P_t), Vp increases remarkably with confining pressure, and at confining pressures higher than P_t, Vp is almost constant or increases slightly with confining pressure. The values of P_t are about 300 bars for CGM and 700-800 bars for FGM.

It can be seen from Fig. 4 and Fig. 5 that volumetric strains show the non-linear changes, and that the crack closure is not effective to the volumetric strain above the P_t. The non-linear change of a volumtric strain at low confining pressure was inferred by Walsh (1965 a) to be caused by the closing of cracks in a rock. Therefore it is inferred from these results that the obtained Vp change is caused by the closing of cracks in a rock.

(ii) Deformation of a Crack due to Confining Pressure

We will attempt to interpret the obtained Vp change due to confining pressure. A shape of a crack in a rock is assumed to be approximated by an oblate spheroid. An explicit expression for the deformation of the oblate spheroidal crack embedded in an infinite isotropic medium subjected to confining pressure can be derived from the general formula which is given by Eshelby (1957) for the deformation of an ellipsoidal inclusion embedded in an infinite isotropic medium subjected to a general stress field.

The displacement in the inclusion, which is embedded in the medium subjected to the uniform applied strain e^A_{ij}, is expressed as

$$u^C_i=(S_{ijkl}e^T_{kl}+\Pi_{ijkl}e^T_{kl})x_j, \tag{3.1.1}$$

where S_{ijkl} and Π_{ijkl} are the coefficients related to the shape of the ellipsoid and the elastic moduli of the medium (see Eshelby, 1957), e^T_{kl} $(=A_{klmn}e^A_{mn})$ the stress-free strain of the equivalent transformed inclusion and X_j the Cartesian coor-

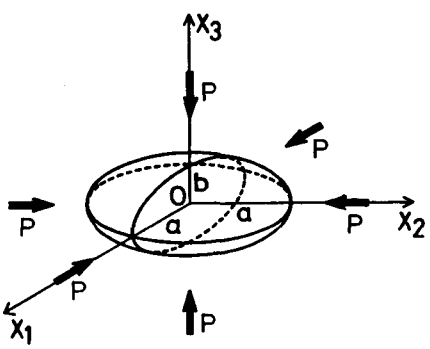

Fig. 3 Coordinate system for the oblate spheroidal crack. The applied pressure P is also shown.

coordinates of a point in the inclusion. The A_{klmn} is a function of the shape of the ellipsoid and the elastic moduli of both inclusion and medium surrounding the inclusion.

For dry cracks, the elastic moduli in the inclusion may be assumed to be zero. We call this inclusion an 'OS crack'. The applied strain and stress field in a coordinate system shown in Fig. 3 is expressed in terms of confining pressure, P, as follows:

$$\left.\begin{aligned} e^A_{11}=e^A_{22}=e^A_{33}&=-P/3K,\\ p^A_{11}=p^A_{22}=p^A_{33}&=-P,\end{aligned}\right\} \qquad (3.1.2)$$

and otherwise is zero,

where K denotes the crack-free bulk modulus of the medium. From equation (3.1.1), we can obtain the surface displacement of the OS crack subjected to P as

$$\left.\begin{aligned} u^C_3&=-(\beta-1)\frac{P}{3K}\mathrm{X}_3,\\ u^C_\rho&=\left[1-\frac{\beta(1-S_{33})-1}{2S_{31}}\right]\frac{P}{3K}\rho,\end{aligned}\right\} \qquad (3.1.3)$$

where

$$\beta=\frac{1-S_{11}-S_{21}+2S_{31}}{(1-S_{33})(1-S_{11}-S_{21})-2S_{13}S_{31}}$$

with Voigt notation; for example, $S_{11}=S_{1111}$. Explicit expressions for S_{ij} are given in appendix A. The shape of the OS crack is prescribed completely by the aspect ratio, which is defined as $\alpha=b/a$ (<1).

For convenience, we reexpress the deformation in terms of the aspect ratio, α, and the crack radius, a. Let α^0 $(=b^0/a^0)$ be the initial aspect ratio and a^0 the initial crack radius. The aspect ratio α and the crack radius a after deformation are derived from equation (31.3) as

and

$$\alpha=\alpha^0\frac{1-(\beta-1)\frac{P}{3K}}{1+\left[1-\frac{\beta(1-S_{33})-1}{2S_{31}}\right]\frac{P}{3K}}, \qquad (3.1.4)$$

$$a=a^0\left[1+\left\{1-\frac{\beta(1-S_{33})-1}{2S_{31}}\right\}\frac{P}{3K}\right]. \qquad (3.1.5)$$

These equations (3.1.4) and (3.1.5) will be used in the following section.

(iii) Inversion of Compressional Wave Velocities for Distribution of Shapes of Cracks in a Rock

Compressional wave velocity increases with confining pressure. This increase can be explained by gradual closing of cracks in a rock (Toksöz et al.,

1976; Cheng and Toksöz, 1979). As confining pressure increases, the thinner cracks close first and the thicker ones become thinner, and will close finally at higher confining pressure. If the compressional wave velocities are obtained as a function of confining pressure, the distribution of the shapes of cracks (DSC) can inversely be obtained from these corpmessional wave velocities. Cheng and Toksöz (1979) discussed a relation between DSC and Vp based on the stattering theory. Here we reconstruct the same relation based on Eshelby's theory.

For a two-phase material with crack-free moduli K and G, inclusion moduli K' and G', and a porosity of the oblate spherodial inclusion with aspect ratio α, $\phi(\alpha)$, Wu (1966) gave the following expressions for the effective moduli K^* and G^* as

$$\left.\begin{aligned}\frac{1}{K^*}&=\frac{1}{K}\left[1+\frac{\phi}{3}T_K\frac{K-K'}{K^*}\right],\\ \frac{1}{G^*}&=\frac{1}{G}\left[1+\frac{\phi}{5}T_G\frac{G-G'}{G^*}\right],\end{aligned}\right\} \tag{3.1.6}$$

where T_K and T_G are scalar functions of K^*, G^*, K', G' and their explicit expressions are given in appendix B.

Cracks would show interaction with each other; that is, the shape of a crack is affected by the stress field produced by the other cracks as well as that produced by the external force. The interaction may affect the elastic moduli. The effective moduli K^* and G^* in equation (3.1.6) include the interaction. For dry cracks, $K'=0$ and $G'=0$, equation (3.1.6) is reduced to the following equation:

$$\left.\begin{aligned}K^*&=K\left(1-\frac{\phi}{3}T_K\right),\\ G^*&=G\left(1-\frac{\phi}{5}T_G\right).\end{aligned}\right\} \tag{3.1.7}$$

The effective moduli K^* and G^* for dry cracks are obtained from equation (3.1.7) using the self-consistent method. Such a low porosity rock as used in this study may have fewer instances of crack interaction; that is, K^* and G^* involved in T_K and T_G in equation (3.1.7) can be approximated by K and G, respectively.

We assume that there are OS cracks with N kinds of aspect ratios in a rock at a differential stress of zero. Then equation (3.1.7) is rewritten as

$$\left.\begin{aligned}K^*&=K\left\{1-\frac{1}{3}\sum_n\phi(\alpha_n)T_K(\alpha_n)\right\},\\ G^*&=G\left\{1-\frac{1}{5}\sum_n\phi(\alpha_n)T_G(\alpha_n)\right\},\end{aligned}\right\} \tag{3.1.8}$$

where $\phi(\alpha_n)$ is the porosity of the n-th crack with aspect ratio α_n. The

effective compressional wave velocity, Vp^*, is defined in terms of the effective moduli as

$$Vp^*=\left[\frac{K^*+\frac{4}{3}G^*}{\rho^*}\right]^{\frac{1}{2}} \tag{3.1.9}$$

Here ρ^* is the effective density defined as

$$\rho^*=\rho(1-\phi^0) \tag{3.1.10}$$

with

$$\phi^0=\sum_n \phi(\alpha_n), \tag{3.1.11}$$

where ρ and ϕ^0 are the crack-free density of the medium and the total porosity, respectively. Substituting K^* and G^* in equation (3.1.8) into equation (3.1.9), the following equation is derived for the effective compressional wave velocity,

$$1-\left(\frac{Vp^*}{Vp^0}\right)^2=\sum_{n=1}^{N}\left[\frac{1}{3K+4G}\{KT_K(\alpha_n)+\frac{4}{5}GT_G(\alpha_n)\}-1\right]\phi(\alpha_n). \tag{3.1.12}$$

where $Vp^0\left(=(K+\frac{4}{3}G/\rho)^{1/2}\right)$ is the crack-free compressional wave velocity.

To obtain the change of Vp^* with confining pressure, the effect of closing of cracks due to the confining pressure should be taken into account because the total porosity for the rock also changes with confining pressure. A porosity of cracks with the aspect ratio α_n^0 at a confining pressure is given from equations (3.1.4) and (3.1.5) as

$$\phi(\alpha_n^0, P_m)=\phi(\alpha_n^0)h(\alpha_n^0, P_m),$$

$$h(\alpha_n^0, P_m)=\left[1-(\beta-1)\frac{P_m}{3K}\right]\left[1+\left\{1-\frac{\beta(1-S_{33})-1}{2S_{31}}\right\}\frac{P_m}{3K}\right]^2, \tag{3.1.13}$$

where α_n^0 is the aspect ratio of n-th crack at a confining pressure of zero and P_m is m-th confining pressure. By taking account of the effect of closing of cracks (i.e., equation (3.1.13)), the effective compressional wave velocity at P_m, Vp_m^*, is expressed as

$$1-\left(\frac{Vp_m^*}{Vp^0}\right)^2=\sum_{n=1}^{N}\left[\frac{1}{3K+4G}\left\{PT_K(\alpha_n^m)+\frac{4}{5}GT_G(\alpha_n^m)\right\}-1\right]h(\alpha_n^0, P_m)\phi(\alpha_n^0), \tag{3.1.14}$$

where α_n^m is the aspect ratio of n-th crack at P_m. Confining pressure changes not only aspect ratio but also crack radius; therefore the effective compressional wave velocity should be also affected by the change of crack radius, which was however ignored by Cheng and Toksöz (1979).

A porosity of cracks with the aspect ratio α^0 is obtained from equation (3.1.14) using the inversion technique, which was also used by Cheng and Toksöz (1979). Equation (3.1.14) is of the form $y=Ax$. If we have M data of Vp^* at different confining pressures, the dimension of the data vector y is M. The

dimension of the model vector x is $N-1$, because there is a constraint given by equation (3.1.11); that is, the sum of the porosity for each aspect ratio must be equal to the total porosity of the rock ϕ^0. The coefficient matrix A is thus the order M by $N-1$. If the number of observed data, M, is greater than that of the aspect ratios, N, the equation $y=Ax$ is an over-determined system of linear equations. We solve this equation by constructing the damped least-squares inverse A_d^{-1} given by Franklin (1970),

$$A_d^{-1}=(A^TA+\varepsilon^2I)^{-1}A^T, \tag{3.1.15}$$

where A^T is the transposed matrix of A, I the unit matrix of the same order as A^TA and ε an adjustable parameter relating to the smallest eigenvalue of A^TA. We will obtain the porosity for each aspect ratio from the Vp^* data by the operation given in equation (3.1.15). The method of determining the DSC in this way is called a linear inversion.

To obtain the most appropriate solution for $\phi(\alpha^0)$, we use a linearized iterative inversion technique. This technique is based on the following expression:

$$\left(\frac{Vp_m^*}{Vp^0}\right)^2-\left(\frac{Vp_m^{*0}}{Vp^0}\right)^2=\sum_{n=1}^{N}\left[1-\frac{1}{3K+4G}\left\{KT_K(\alpha_n^m)+\frac{4}{5}GT_G(\alpha_n^m)\right\}\right] \cdot h(\alpha_n^0, P_m)\Delta\phi(\alpha_n^0) \tag{3.1.16}$$

where Vp_m^{*0} is the effective compressional wave velocity calculated for the initial guess model at P_m and $\Delta\phi(\alpha_n^0)$ the small difference of $\phi(\alpha^0)$. For equation (3.1.16), we have the following constraint:

$$\sum_{n=1}^{N}\Delta\phi(\alpha_n^0)=0. \tag{3.1.17}$$

which is different from that for the linear inversion (i.e., equation (3.1.11)). The solution of the linear inversion, $\phi(\alpha_n^0)$, is used as an initial guess model for the linearized iterative inversion. Since the effective compressional wave velocities calculated from the solution obtained by the linearized iterative inversion technique fit the observed ones better than those by the linear inversion technique, the solution obtained by the former technique is considered to be more appropriate than that by the latter technique. Therefore the DSC obtained by the former technique will be discussed in the following section.

Reliability of the results thus obtained can be examined by comparing the calculated strains with the observed ones. The volumetric strain at P_m can be calculated by the following equation:

$$\left(\frac{\Delta V}{V}\right)_m=\int_0^{P_m}\frac{dP}{K^*(P)}, \tag{3.1.18}$$

where $K^*(P)$ is the effective bulk modulus calculated from equations (3.1.8) and

(3.1.13).

(iv) Distribution of the Shapes of Cracks in two Calcareous Rocks

The calculated compressional wave velocities and volumetric strains are shown as a function of confining pressure in Fig. 4 for CGM and in Fig. 5 for FGM, in which the measured ones are also shown. The measured *Vp* are scattered to some extrent. The scattering is mainly due to using different samples. The measured *Vp* were bounded with two curves which represent the upper and lower limits of the scattering, so that the two curves may give the range of errors in measurements and the difference of DSC between different samples. The two curves are called the upper curve and the lower curve, respectively. To examine the effect of the scattering on the solution of the

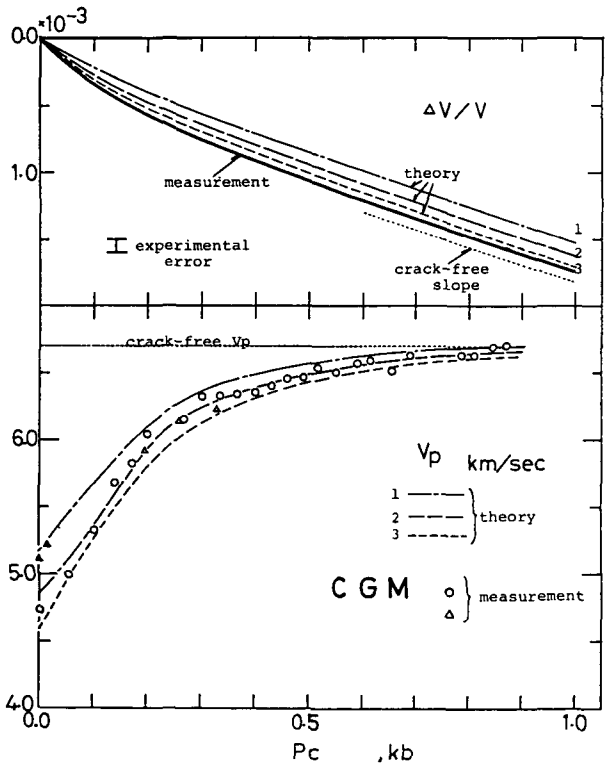

Fig. 4 Measured Vp and strain changes and calculated ones due to confining pressure for CGM. The measured Vp for different samples are shown by different symbols and the measured volumetric strain by a thick solid line. Calculated Vp and strain changes using three kinds of DSC shown in Fig. 6 are shown by different lines. The numbers attached to these calculated curves in this figure correspond to those in Fig. 6.

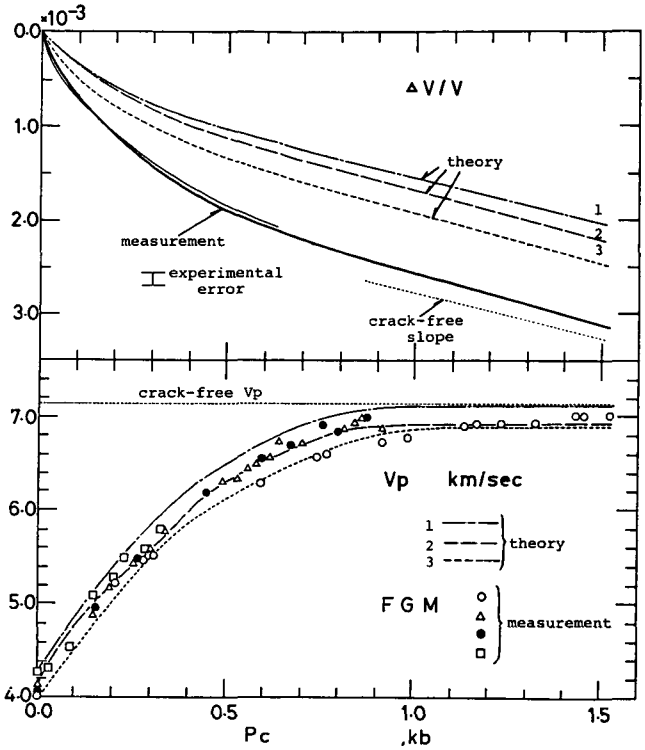

Fig. 5 Same as in Fig. 4 for FGM. Calculated Vp and strain changes were based on three kinds of DSC shown in Fig. 7.

inversion, we prepared three sets of Vp data as follows: all measured data (set I); interpolated Vp data sampled from the upper curve at the same increment of confining pressure (set II); and, interpolated Vp data sampled from the lower curve at the same increment of confining pressure (set III).

The solutions of the inversion for these three sets of data are shown as line spectra of aspect ratio in Fig. 6 for CGM and Fig. 7 for FGM. In calculations for all the sets, the damping factor ε introduced in equation (3.1.15) was taken to be one. Spectral amplitude for each aspect ratio in these figures corresponds to the porosity which is occupied by cracks having an aspect ratio. The crack porosities obtained for the three sets of data are almost the same with each other where the aspect ratio is less than 10^{-3}, but those where the aspect ratio is larger than 10^{-3} are different from each other. The good agreement between the calculated Vp for set I and the measured Vp is obtained; the measured Vp is between the calculated Vp for set II and that for set III.

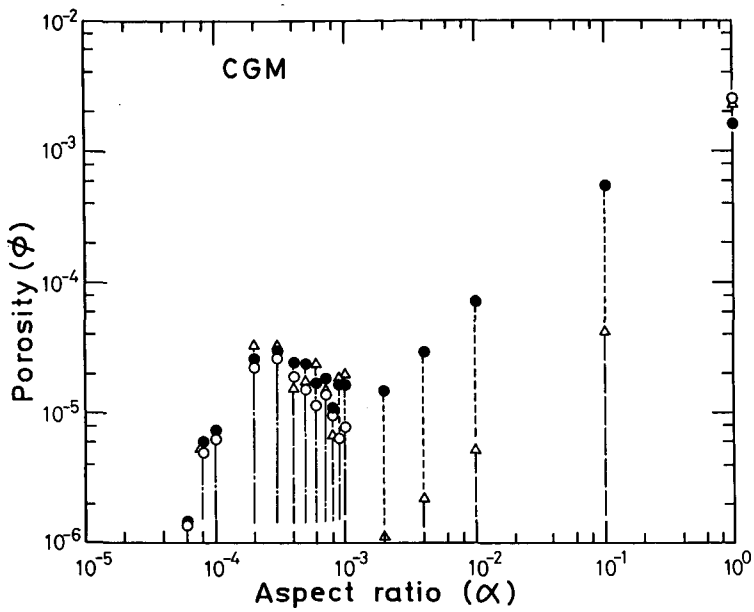

Fig. 6 Porosity distribution versus aspect ratio of cracks for CGM. The distributions determined from three data sets, which were made of all measured data and two kinds of interpolated data, respectively, are shown by different symbols.

To investigate the difference of the measured results between both rocks mentioned in previous section 3.1-(i), we will compare the DSC for CGM with that for FGM. The average DSC for each rock was constructed from the three solutions obtained by the inversion technique and is shown as the continuous spectra in Fig. 8. This figure shows that DSC's for two kinds of rocks are different from each other in three ways: 1) the total crack porosity for FGM is larger than that for CGM, 2) there is one peak in each DSC and the aspect ratio for each peak is about $1-3\times10^{-4}$ for CGM and $5-9\times10^{-4}$ for FGM, 3) and, the crack porosity for CGM is larger than that for FGM when $\alpha<4\times10^{-4}$, and that for FGM is larger than that for CGM when $\alpha>4\times10^{-4}$. The confining pressure at which the cracks with the aspect ratio given in 2) will close almost coincides with P_t. Nur and Simmons (1969) measured compressional wave velocities at confining pressure up to 3 kbars for six kinds of rocks (two kinds of limestone, a dolomite, three kinds of granite) which are presented in Table 1 in their paper. We calculated also the DSC for the rocks used by Nur and Simmons (1969). As a result, it was obtained that there was one peak in each DSC, and the aspect ratio for each peak was different.

The calculated volumetric strains shown in Fig. 4 and Fig. 5 are under-

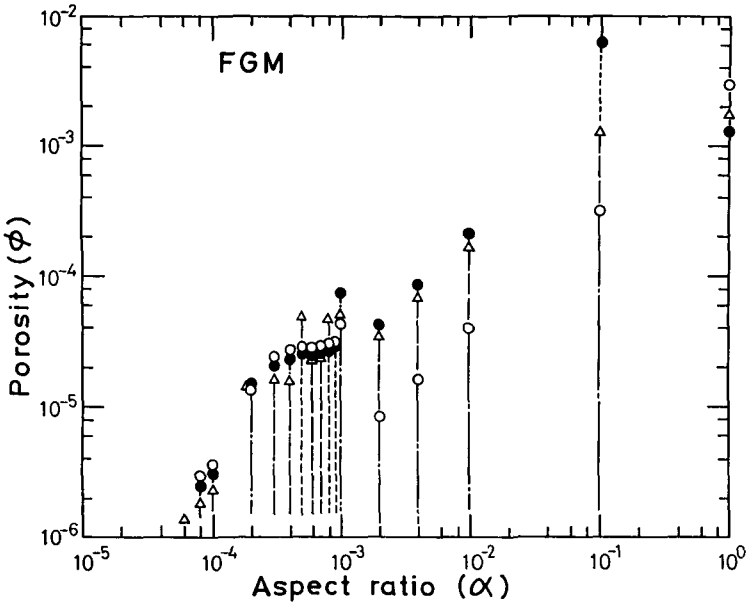

Fig. 7 Same as in Fig. 6 for FGM.

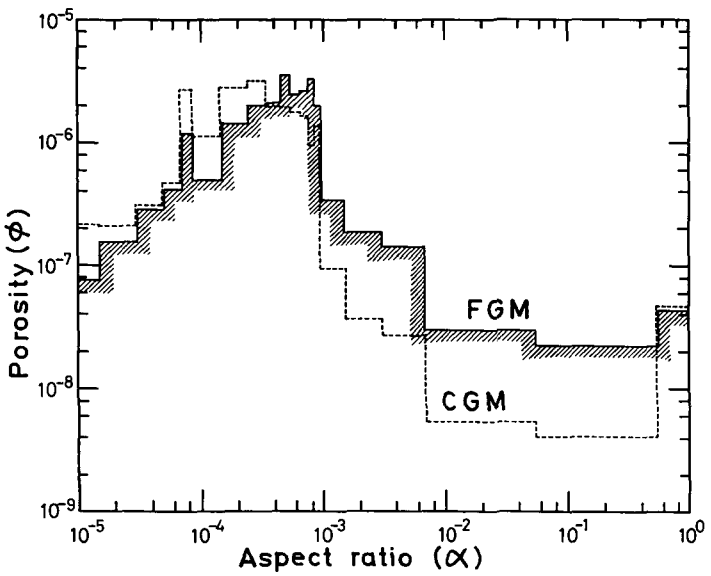

Fig. 8 Comparison of continuous porosity distributions versus aspect ratios of cracks for CGM and FGM. These distributions are drawn up as the average of the results in Fig. 6 and Fig. 7. Note that distributions for both rocks are clearly different from each other.

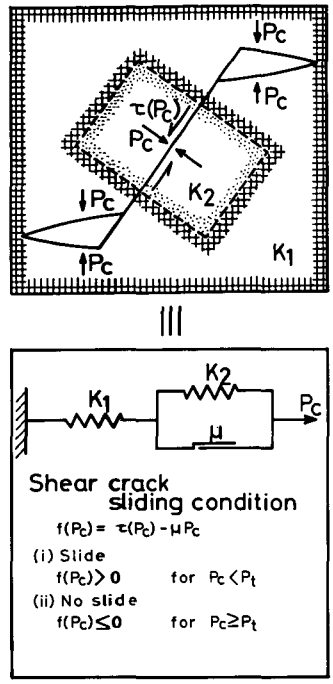

Fig. 9 The effect of shear cracks on the elastic moduli under confining pressure. A sliding crack model is schematically shown in the upper figure, a rheological model which is equivalent to it is also shown in the lower figure.

underestimate for both rocks. The difference between the calculated and measured volumetric strains for FGM is greater than that for CGM. For CGM, the difference is within the experimental error. This result is consistent with that obtained by Simmons and Brace (1965). According to them, the dynamic moduli of some igneous rocks are about two times greater than the static ones at atmospheric pressure, and the difference between the dynamic and static moduli decreases as confining pressure increases. The difference may be due to the sliding of shear cracks.

Now we will consider the effect of the shear cracks on the elastic moduli. Although an isolated shear crack is not deformed under confining pressure, a shear crack connected to tensile cracks may be deformed by the shear stress generated by the deformation of the tensile cracks. This is shown in Fig. 9. Since such a low stress disturbance as elastic waves gives no deformation to the shear crack, the dynamic moduli K_d are not affected by shear cracks. We assume that the static moduli K_s are affected by shear cracks at a confining

pressure lower than P_t, while those at a confining pressure higher than P_t are little affected by shear cracks because of the sufficiently high normal stress. Thus the following stress-strain relations are obtained,

$$e=\frac{K_1+K_2}{K_1K_2}Pc \qquad \text{for } Pc<P_t,$$

$$e=\frac{Pc}{K_1} \qquad \text{for } Pc>P_t.$$

Here K_d equals to K_1 under confining pressure and K_s at confining pressures lower thas P_t equals to $K_1K_2/(K_1+K_2)$. Therefore the ratio K_s to K_d at confining pressures lower than P_t is less than one. If this ratio is assumed to be 0.53 for FGM, the observed volumetric strain also can be explained well as shown by the thin solid line in Fig. 5.

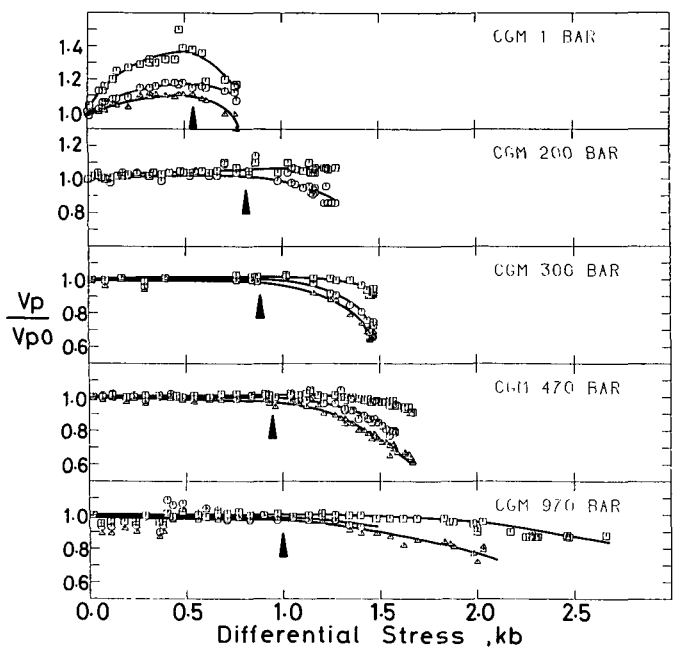

Fig. 10 Vp's in different three directions plotted against differential stress with different symbols (□ ; almost parallel to the load axis, ○ ; oblique to the load axis, △ ; perpendicular to the load axis) for CGM. The number attached to the upper corner of each figure denotes the confining pressure kept at constant during the measurement.

3.2 *Vp Change due to Differential Stress*

(i) Experimental Results

The compressional wave velocities were measured for three directions against different differential stresses at a confining pressure kept at constant. Figure 10 shows the compressional wave velocities measured for CGM and Fig. 11 those for FGM, in which the measured compressional wave velocities are normalized with Vp^0 which is the compressional wave velocity at a differential stress of zero. The amount of scatter of the measured compressional wave velocities for CGM is greater than that for FGM. This may be due to the way of loading (see section 2.3). The volumetric strains for each confining pressure were also measured as a function of differential stress, and are shown in Fig. 12 for CGM and in Fig. 13 for FGM. The onset stress of dilatancy, P_d, which is defined from a stress-strain curve in the usual manner (e.g., Brace et al., 1966),

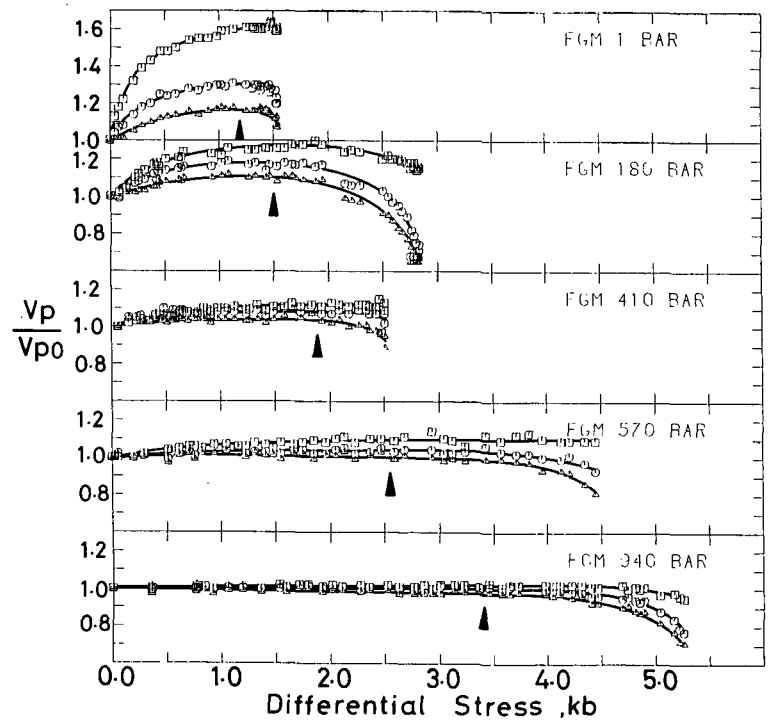

Fig. 11 Same as in Fig. 10 for FGM. A difference between the maximum and minimum Vp at low differential stress decreases gradually with increasing confining pressure, but in Fig. 10, the difference decreases rapidly with increasing confining pressure.

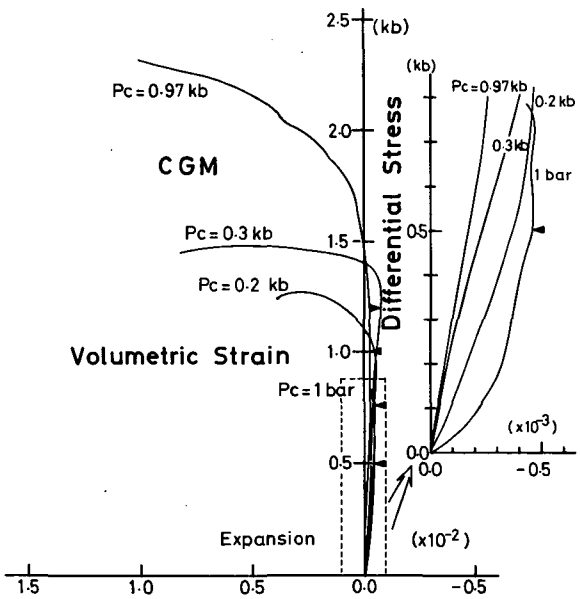

Fig. 12 Volumetric strains versus differential stress under a confining pressure for CGM. The inset denotes the magnified stress-strain curves at low differential stress. Solid triangles denote onset stresses of dilatancy. The onset stresses were determined by the usual method.

is shown by a solid triangle in Fig. 12 and Fig. 13. The volumetric strains show more or less non-linear changes, that is, volume reductions due to compaction, before the onset of dilatancy for all the confining pressures measured. The changes were inferred by Walsh (1965 b) to be caused by the closing of cracks in a rock.

We define the amount of anisotropy of compressional wave velocity, Va, as follows:

$$Va=\frac{Vp''-Vp^{\perp}}{\bar{V}p}, \tag{3.2.1}$$

where $\bar{V}p$ is the average Vp of compressional wave velocities in three directions, Vp'' and $Vp^{\perp}$ are the compressional wave velocities in the directions parallel and perpendicular to the load axis, respectively. From the changes of Va and $\bar{V}p$ measured, we can obtain features of the Vp change under differential stress in detail. The amount of anisotropy of compressional wave velocity (Va) and the average compressional wave velocity ($\bar{V}p$) against differential stress (σ) and those against volumetric strain (DV/V) are shown in Fig. 14 to Fig. 18 for CGM and in Fig. 19 to Fig. 23 for FGM. The onset stress

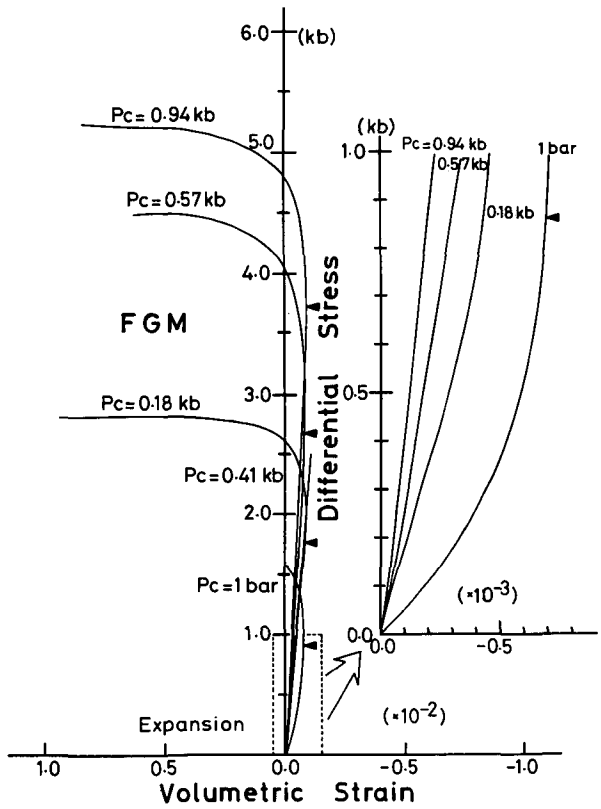

Fig. 13 Same as in Fig. 12 for FGM.

of dilatncy, p'_d, which is defined graphically from a stress-anisotropy curve as shown in Fig. 25, is shown by an arrow in these figures. The Va at a differential stress of zero is less than 5% for each rock under atmospheric pressure.

The measured results may be summarized as follows:

1) As the differential stress increases before the onset of dilatancy under atmospheric pressure, Vp'' for CGM increases by 36% which gives the maximum Vp'' for CGM; Vp'' for FGM by 60% which also gives the maximum Vp'' for FGM; $Vp^{\perp}$ for CGM by 10% which gives the maximum $Vp^{\perp}$ for CGM; and, $Vp^{\perp}$ for FGM by 17% which gives the maximum $Vp^{\perp}$ for FGM (Fig. 10, Fig. 11). This is consistent with the results obtained for different rock specimens under uniaxial compression by Tocher (1957), Nur and Simmons (1969 a) and Fujii and Hamano (1977).

2) For all the confining pressures measured, $Vp^{\perp}$ decreases drastically with

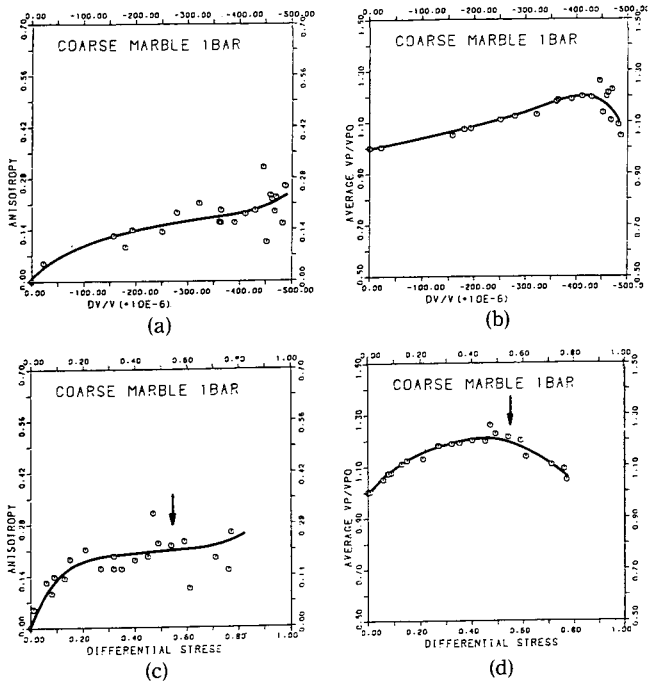

Fig. 14 Vp anisotropy (Va) and average Vp ($\bar{V}p$) versus differential stress and volumetric strain under a confining pressure of 1 bar (Pc=1 bar) for CGM. (a): Va versus volumetric strain, (b): $\bar{V}p$ versus volumetric strain, (c): Va versus differential stress, (d): $\bar{V}p$ versus differential stress. A curve which smoothes the measured data is also shown by a solid line in each figure. Arrows shown in figures (c) and (d) denote an onset stress of dilatancy. The onset stress is determined from the smoothed curve for the relation between Va and differential stress.

increasing differential stress during dilatancy (Fig. 10, Fig. 11). This is consistent with the results obtained for different rock specimens at a confining pressure of 1 bar by Gupta (1973), at a confining pressure of 0.5 Kbars by Lockner et al. (1977) and at confining pressures of 0.5 and 1.0 Kbars by Soga et al. (1978).

3) The directional dependence of Vp is approximately expressed as a function of $\cos 2\theta$ for all the confining pressures measured, where θ is an angle between the direction of propagation and that of the load axis (Fig. 10, Fig. 11). This is consistent with the results obtained for different rock specimens under uniaxial compression by Nur and Simmons (1969).

4) When $\sigma < P_d'$, Va at the same differential stress decreases rapidly for CGM and gradually for FGM with increasing confining pressure (Fig. 10, Fig. 11).

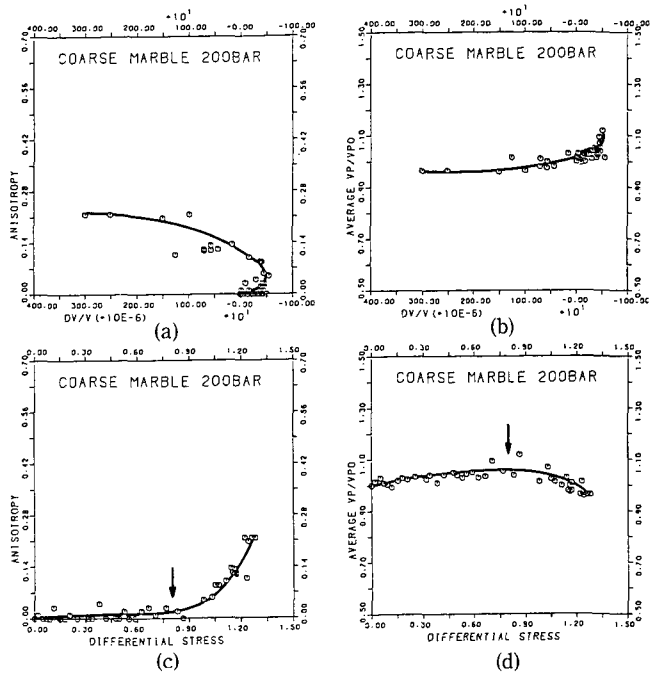

Fig. 15 Same as in Fig. 14 at Pc=200 bars for CGM.

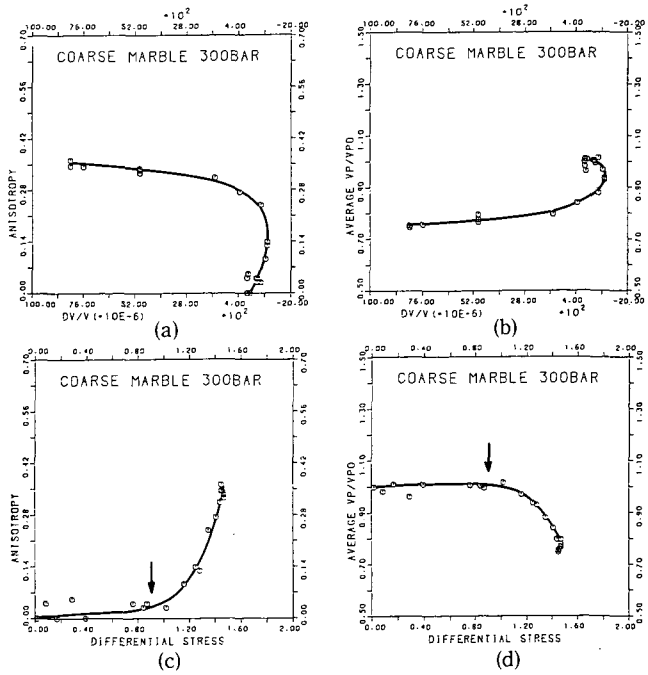

Fig. 16 Same as in Fig. 14 at Pc=300 bars for CGM.

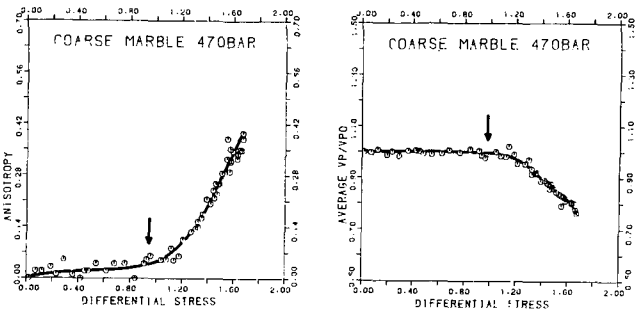

Fig. 17 Same as in Fig. 14 at Pc=470 bars for CGM. However, the Va and $\bar{V}p$ changes against volumetric strain are not shown because of no data of volumetric strain due to sensor trouble.

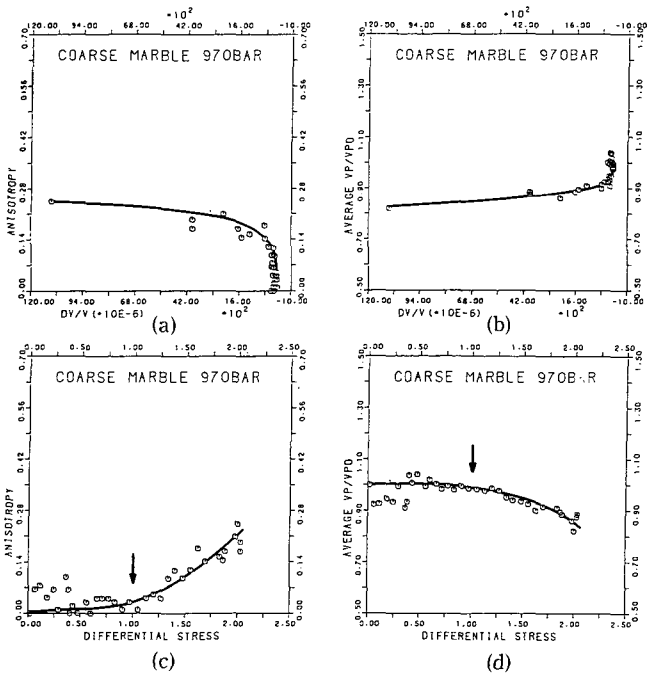

Fig. 18 Same as in Fig. 14 at Pc=970 bars for CGM.

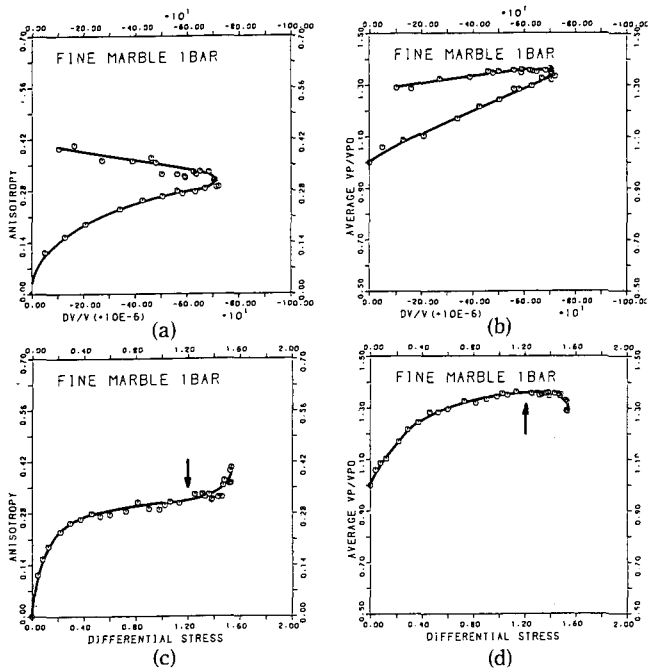

Fig. 19 Same as in Fig. 14 at Pc=1 bar for FGM.

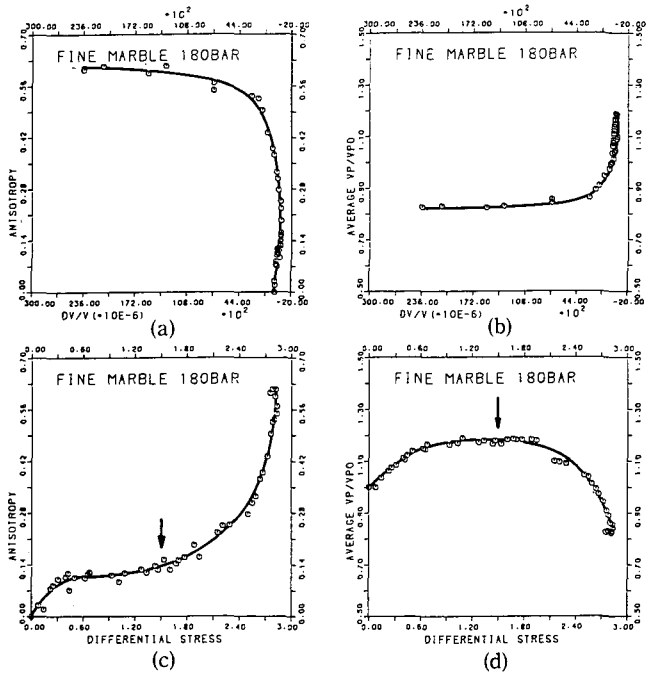

Fig. 20 Same as in Fig. 14 at Pc=180 bars for FGM.

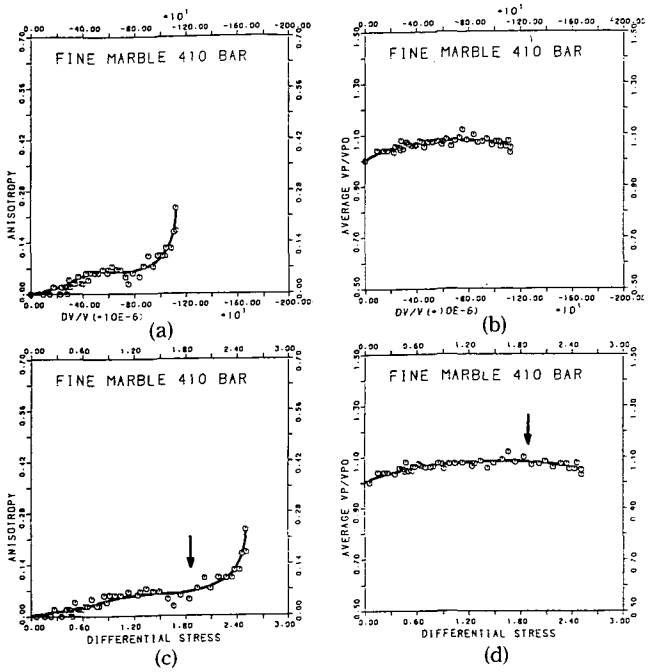

Fig. 21 Same as in Fig. 14 at Pc=410 bars for FGM.

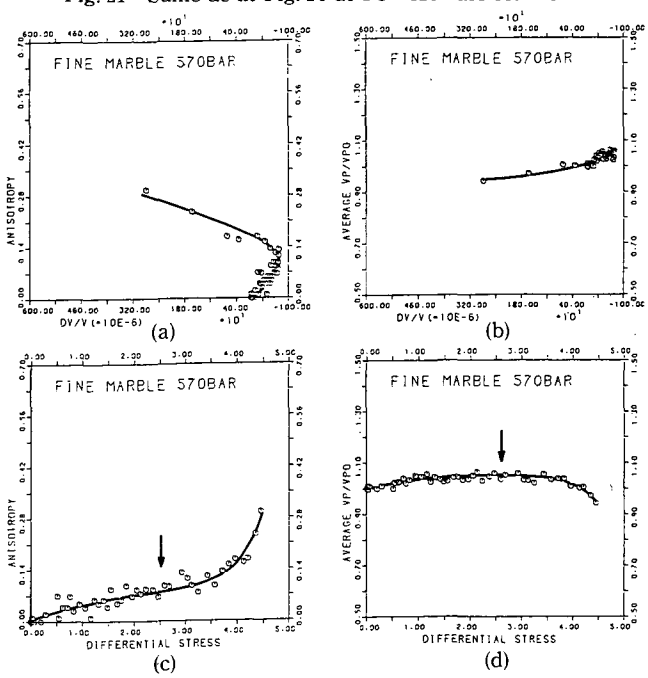

Fig. 22 Same as in Fig. 14 at Pc=570 bars for FGM.

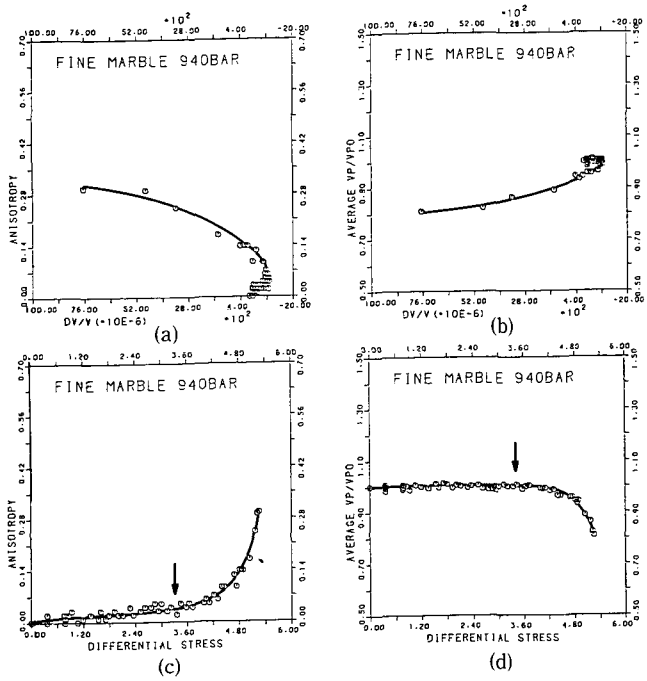

Fig. 23 Same as in Fig. 14 at Pc=940 bars for FGM.

5) When $\sigma < P_d'$, Va increases with increasing differential stress and reaches its maximum (Va^{max}) at a differential stress. By contrast, when $\sigma > P_d'$, Va increases exponentially with increasing differential stress. This Va increase occurs at all the confining pressures measured (Fig. 10, Fig. 11 and Fig. 14 to Fig. 23).

6) As confining pressure increases, Va^{max} decreases rapidly for CGM and gradually for FGM ; Va^{max} for both samples show an exponential decrease with increasing confining pressure (Fig. 24). Va^{max} for FGM is larger than that for CGM at all the confining pressures.

7) Va^{max} at a certain confining pressure is almost linearly related to the increase of initial Vp from a confining pressure of zero up to the confining pressure (Fig. 38). Here the initial Vp is the Vp at a differential stress of zero.

8) When $\sigma < P_d'$, $\bar{V}p$ always increases (Fig. 14 to Fig. 23).

9) When $\sigma > P_d'$, $\bar{V}p$ always decreases (Fig. 14 to Fig. 23).

10) When $\sigma < P_d$, the rates of Va and $\bar{V}p$ change are large while the change of volume reduction is small. By contrast, when $\sigma > P_d$, those are small while the change of volume expansion is large and decrease with increasing volumetric

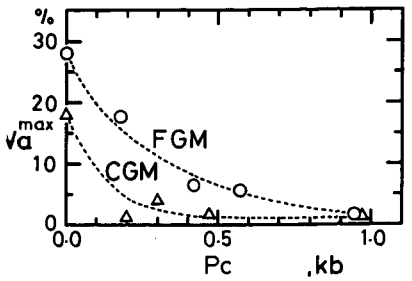

Fig. 24 Maximum Va due to compaction versus confining pressure. For both rocks, the maximum Va show an exponential decrease with increasing confining pressure.

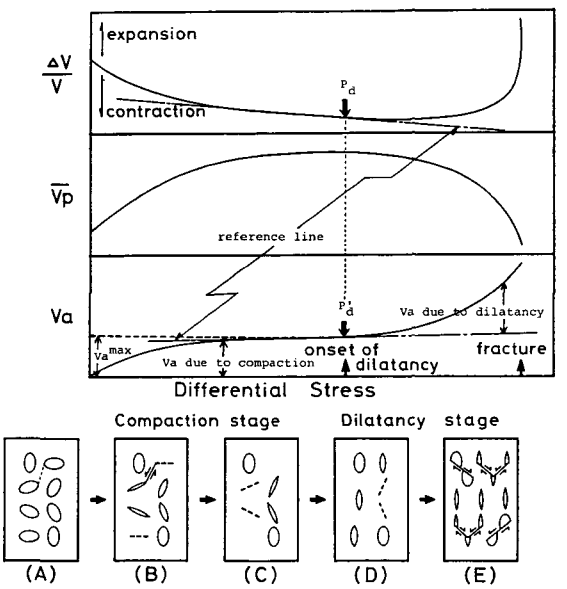

Fig. 25 Schematic relationship among Va, $\bar{V}p$ volumetric strain and differential stress under a confining pressure and the deformation process of rocks. The onset stresses P_d and P'_d are determined graphically from a stress-strain curve and from a stress-anisotropy curve, respectively. The deformation process is as follows: rocks are initially isotropic (stage (A)). Since cracks are closed by differential stress, Va and $\bar{V}p$ increase (stage (B)), and reach those maximum (stage (C)). Since cracks are generated, Va and volumetric strain increase and $\bar{V}p$ decrease (stage (D)). Cracks may begin to connect with each other (stage (E)).

strain (Fig. 14 to Fig. 23).

11) A rate of the compaction decreases rapidly for CGM and gradually for FGM with increasing confining pressure (Fig. 12, Fig. 13). This is consistent

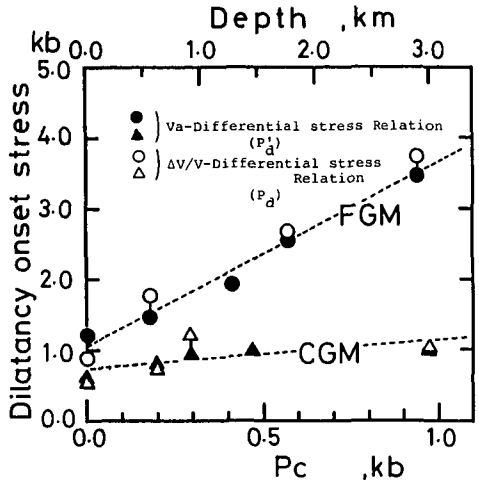

Fig. 26 Dilatancy onset stresses versus confining pressure. The onset stresses were determined in two ways: one was determined from a strain-stress relation; and the other from a Va-stress relation. Note that the onset stresses from the Va-stress relations almost coincide with ones from the strain-stress relations. Depth calculated by assuming a density is also shown in the axis of abscissa.

with the result 4).

12) The P'_d almost coincides with the P_d (Fig. 26).

13) The P'_d increases linearly with increasing confining pressure up to 1 Kbars (Fig. 26). Increasing rate of P'_d for FGM is larger than that for CGM.

From the results 1), 4), 5), 8) and 11), we can conclude that the cause of the anisotropy of Vp at $\sigma < P'_d$ is the closing of cracks in a rock. Therefore, we call this anisotropy of Vp 'VA due to compaction'. From the results 2), 5), 9) and 12), we can conclude that the cause of the anisotropy of Vp at $\sigma > P'_d$ is the generation of dilatant cracks in a rock. Therefore, we call this anisotropy of Vp 'VA due to dilatancy'. The onset stress of dilatancy, P'_d, corresponds to the transitional stress from VA due to compaction to VA due to dilatancy. Even when it is difficult to determine the onset stress of dilatancy from a stress-strain curve for uniaxial compression (Fig. 12, Fig. 13), our method based on a stress-Va curve could easily give the onset stress. Comparison of the result 1) with the results shown in Fig. 4 and Fig. 5 shows that Vp'' change caused by the differential stress is similar to Vp change caused by the confining pressure; that is, the effect of the differential stress on Vp'' is equivalent to that of the confining pressure on Vp. The differences between the results for both rocks (i.e., results 4), 6) and 11)) are due to the difference between the DSC's for both rocks. The

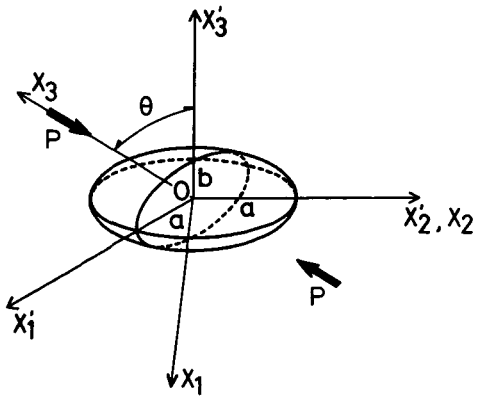

Fig. 27 Two kinds of coordinate systems associated with crack geometry and applied stress field. The former system corresponds to a primed one (X'-system), and the latter system a non-primed one (X-system).

results 8) and 9) indicate that by observing Va and $\bar{V}p$, we can determine whether VA is caused by the compaction or by the dilatancy.

(ii) Deformation of a Crack due to Differential Stress

We will attempt to interpret the obtained anisotropic change of Vp due to differential stress in the following four sections. In this section, an explicit expression for deformation of an OS crack embedded in an infinite isotropic medium subjected to differential stress can be derived from the general formula (i.e., equation (3.1.1)) which is given by Eshelby (1957).

We define two coordinate systems as shown in Fig. 27; one is X-system whose axes coincide with principal ones of a stress field, and the other is X'-system whose axes coincide with ones of the OS crack. Let θ be an angle between the direction of a crack-normal and X_3-axis. We have the following expressions for the applied field in X'-system:

$$\left.\begin{aligned} e^A_{11} &= \frac{P}{E}(\nu \cos^2\theta - \sin^2\theta), \\ e^A_{22} &= \frac{P}{E}\nu, \\ e^A_{33} &= \frac{P}{E}(\nu \sin^2\theta - \cos^2\theta), \\ e^A_{33} &= e^A_{13} = -\frac{P}{2G}\sin 2\theta, \end{aligned}\right\} \qquad (3.2.2)$$

$$\left.\begin{aligned} p^A_{11} &= -P\sin^2\theta, \\ p^A_{33} &= -P\cos^2\theta, \\ p^A_{31} &= p^A_{13} = -\frac{1}{2}P\sin 2\theta, \end{aligned}\right\}$$

where E, G and ν denote the Young's modulus, the shear modulus and the Poisson's ratio of the crack-free medium, respectively, and P is the simple compressive stress.

The surface displacement of an OS crack is obtained from equations (3.1.1) and (3.2.2) as

$$\left.\begin{aligned} u^C_1 &= \left[-\nu+\frac{1-\varepsilon(1-S_{33})}{2S_{31}}+\frac{(1+\nu)\sin^2\theta}{S^0}\{S_{13}(1-S_{11}+S_{21}\right. \\ &\quad +S_{31}(2S_{11}-2S_{21}-1))-(1-S_{33})(S_{11}+(S_{21}+S_{11}) \\ &\quad \left.\cdot(S_{21}-S_{11}))\}\right]\frac{P}{E}\rho-\frac{S_{55}\sin 2\theta}{(1-2S_{55})}\frac{P}{G}x_3', \\ u^C_2 &= \left(-\nu+\frac{1-\varepsilon(1-S_{33})}{2S_{31}}+\frac{(1+\nu)\sin^2\theta}{S^0}\left\{S_{13}(1-S_{11}+S_{21}-S_{31})\right.\right. \\ &\quad \left.\left.-(1-S_{33})S_{21}\right\}\right)\frac{P}{E}\rho, \\ u^C_3 &= (1-\varepsilon+(1+\nu)\delta\sin^2\theta)\frac{P}{E}x_3'-\frac{S_{55}\sin 2\theta}{(1-2S_{55})}\frac{P}{G}\rho, \end{aligned}\right\} \quad (3.2.3)$$

where

$$\varepsilon=\frac{1-S_{11}-S_{21}-2\nu S_{31}}{(1-S_{11}-S_{21})(1-S_{33})-2S_{13}S_{31}},$$

$$\delta=\frac{(1-S_{11}-S_{21})S_{33}+S_{31}(2S_{13}-1)}{(1-S_{11}-S_{21})(1-S_{33})-2S_{13}S_{31}},$$

$$S^0=(1-S_{11}+S_{21})\{(1-S_{11}-S_{21})(1-S_{33})-2S_{13}S_{31}\}.$$

When $\theta=0$ and $P=-T$, where T is a simple tension, these expressions are the same as the expressions obtained by Sato (1978), except for the suffixes.

Let $a^0(=b^0/a^0)$ be the initial aspect ratio and a^0 the initial crack radius. The shape of a deformed crack by the differential stress will differ a little from the oblate spheroid. We approximate it by an oblate spheroid to apply the Eshelby's theory. The crack radius after deformation is approximated as

$$\left.\begin{aligned} a &= a^0(1+\bar{e}), \\ \bar{e} &= \frac{1}{2}\left(\frac{\partial u^C_1}{\partial\rho}+\frac{\partial u^C_2}{\partial\rho}\right). \end{aligned}\right\} \quad (3.2.4)$$

and the aspect ratio after deformation is approximated as

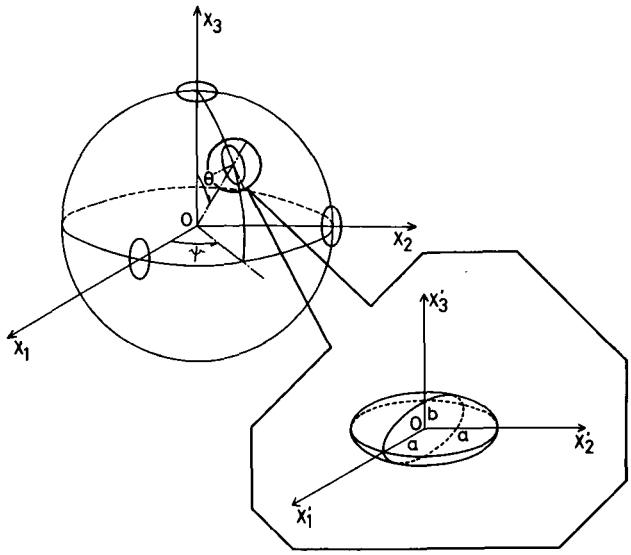

Fig. 28 Relation between X-system whose axes coincide with the principal stress ones and X'-system whose axes coincide with principal ones of an oblate spheroid. Angles θ and ψ prescribing the direction of a crack normal are also shown.

$$\left.\begin{aligned} a &= a^0 \frac{1+e_v}{(1+\bar{e})^3}, \\ e_v &= \frac{\partial u_1^c}{\partial \rho} + \frac{\partial u_2^c}{\partial \rho} + \frac{\partial u_3^c}{\partial x_3'}. \end{aligned}\right\} \qquad (3.2.5)$$

These equations (3.2.4) and (3.2.5) will be used in the following section.

(iii) Theoretical Formulation for Vp in a Medium Containing Cracks

We will derive the explicit expression for the effective elastic constants of an isotropic medium containing randomly and uniformly oriented *OS* cracks. Nur (1971) discussed the orientation of stress-induced cracks and gave the expressions for effective elastic wave velocities in an isotropic medium containing oriented penny-shaped cracks. Anderson et al. (1974) considered the effective elastic wave velocities in an isotropic medium containing aligned *OS* cracks. Garbin and Knopoff (1973) investigated, analytically, the scattering of elastic waves by a penny-shaped crack and derived the expressions for the velocity variation in the zero-frequency limit of elastic waves propagating through an isotropic medium containing parallel penny-shaped cracks dilutely distributed.

We will now start from the general expression of the interaction energy

given by Eshelby (1957). We consider an isotropic medium with crack-free elastic constants C_{ijkl} (i.e., $C_{iiii}=K+\frac{4}{3}G$, $C_{iijj}=K-\frac{2}{3}G$, $C_{ijij}=G$, otherwise is zero), where dry OS cracks with an aspect ratio α are contained. The interaction energy of an ellipsoidal inclusion with a strain field, which in the absence of the inclusion, would be a uniform strain in an infinite medium, is given as follows:

$$\left.\begin{aligned} E_{int}&=-\frac{1}{2}Vp_{ij}^{A}e_{ij}^{T},\\ p_{ij}^{A}&=C_{ijpq}e_{pq}^{A},\\ e_{ij}^{T}&=A_{ijst}e_{st}^{A},\end{aligned}\right\} \tag{3.2.6}$$

where V is the volume of an OS crack, e_{ij}^{A} the uniform applied strain at infinity, p_{ij}^{A} the applied stress field, and e_{ij}^{T} the stress-free strain of the equivalent transformed inclusion. Here A_{ijst} is a function of the aspect ratio of the crack and the crack-free elastic constants.

We consider a case of dilute concentration of cracks. The medium is divided into small cells each of which contains only one crack. If the cell dimension is sufficiently larger than the crack radius, E_{int} is approximately the interaction energy of the crack in the cell with the strain e_{ij}^{A} that would be produced by the surface tractions applied to the surface of medium occupying the cell. For the cell, we can sum up the E_{int} to form the entire interaction energy of the medium. Since the low porosity rocks used in this study may be considered as consisting of these cells, the effective elastic energy per unit volume is given as

$$E^{*}=\frac{1}{2}e_{ij}^{A}e_{kl}^{A}(C_{ijkl}-\phi C_{ijpq}A_{pqkl}), \tag{3.2.7}$$

where ϕ is a porosity of cracks.

We assume that there are cracks with N kinds of aspect ratios at a differential stress of zero in every direction which is described by θ and ψ as shown in Fig. 28. When the crack inclines, A_{pqkl} in the second term of equation (3.2.7) is transformed by the fourth order tensor as

$$A_{pqkl}(\alpha,\ \theta,\ \psi)=A_{pqkl}L_{pp'}L_{qq'}L_{kk'}L_{ll'} \tag{3.2.8}$$

where L_{ij} are the direction cosines determined by θ and ψ.

Since the volume of an OS crack is $\frac{4}{3}\pi\alpha a^{3}$ (a is the half length of major axis of an oblate spheroid), the porosity of the cracks whose normals are in the region between θ and $\theta+d\theta$, ψ and $\psi+d\psi$ is

$$\phi(\alpha_n,\ \theta,\ \psi)=\frac{4}{3}\pi\alpha_n a^3 D(\alpha_n,\ \theta,\ \psi)\sin\theta d\theta d\psi, \tag{3.2.9}$$

where $D(\alpha_n, \theta, \psi)$ is the number of cracks with aspect ratio α_n in a unit volume in the direction θ, ψ. The total porosity of the cracks is

$$\phi^0=\frac{4}{3}\pi a^3\sum_{n=1}^{N}\alpha_n\int_0^{2\pi}d\psi\int_0^{\pi}D(\alpha_n,\ \theta,\ \psi)\sin\theta d\theta. \tag{3.2.10}$$

For the cracks assumed, the effective elastic energy per unit volume is rewritten using equations (3.2.8) and (3.2.9),

$$\begin{aligned}E^*=\frac{1}{2}e_{ij}^A e_{kl}^A\Big\{&C_{ijkl}-\frac{4}{3}\pi a^3\sum_{n=1}^{N}\alpha_n\int_0^{2\pi}d\psi\int_0^{\pi}D(\alpha_n,\ \theta,\ \psi)\\&\cdot C_{ijpq}A_{pqkl}(\alpha_n,\ \theta,\ \psi)\sin\theta d\theta\Big\}.\end{aligned} \tag{3.2.11}$$

On the other hand, we have the following relation for a composite medium

$$E^*=\frac{1}{2}C_{ijkl}^* e_{ij}^A e_{kl}^A, \tag{3.2.12}$$

where C_{ijkl}^* are the effective elastic constants of the composite medium. Comparing equation (3.2.11) with equation (3.2.12), we obtain the effective elastic constants of the composite medium;

$$\begin{aligned}C_{ijkl}^*=C_{ijkl}-\frac{4}{3}\pi a^3\sum_{n=1}^{N}\alpha_n\int_0^{2\pi}d\psi\int_0^{\pi}D(\alpha_n,\ \theta,\ \psi)\\\cdot C_{ijpq}A_{pqkl}(\alpha_n,\ \theta,\ \psi)\sin\theta d\theta.\end{aligned} \tag{3.2.13}$$

For the load being applied in the direction of X_3-axis as shown in Fig. 28, only five effective elastic constants, that is, C_{11}^*, C_{33}^*, C_{13}^*, C_{44}^* and $(C_{11}^*-C_{12}^*)/2$ in Voigt notation, are independent (e.g., Love, 1934; Anderson, 1961), where X_3 is the axis of the symmetry of rotation. According to Anderson et al. (1974), the velocity equation in any plane containing the X_3-axis is given in the following form,

$$\left(V-\frac{s^2}{2}X\right)\{(V-s^2W)(V-c^2Z)-s^2c^2Y^2\}=0, \tag{3.2.14}$$

where
$$\begin{aligned}V&=\rho^* v^{*2}-C_{44}^*\\W&=C_{11}^*-C_{44}^*\\X&=C_{11}^*-C_{12}^*-2C_{44}^*\\Y&=C_{13}^*+C_{44}^*\\Z&=C_{33}^*-C_{44}^*\\c&=\cos\theta,\qquad s=\sin\theta.\end{aligned}$$

Here v^* is the effective elastic wave velocity and ρ^* is the effective density given in equation (3.1.10), and c and s prescribe the direction of propagation of an

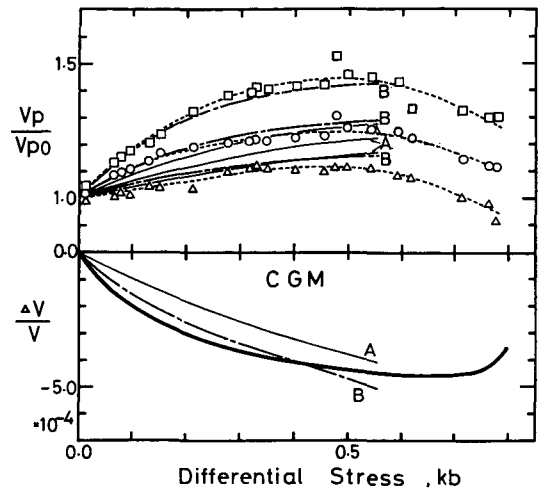

Fig. 29 Calculated Vp and strain changes and measured Vp and strain changes in the stage of compaction at Pc=1 bar for CGM. Curves which smooth the measured Vp data are also shown by broken lines. Calculated values denoted by symbol A are based on the DSC shown in Fig. 6. Calculated values denoted by symbol B are based on the assumption that the initial total porosity is a parameter.

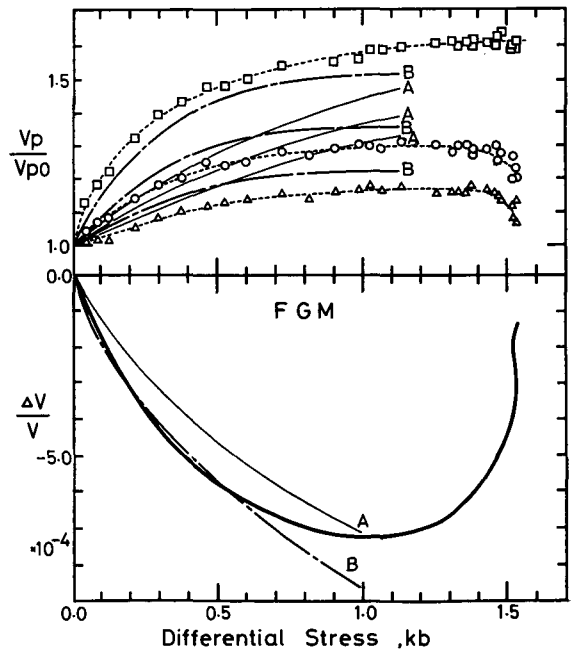

Fig. 30 Same as in Fig. 29 at Pc=1 bar for FGM.

elastic wave; that is, if $c=1$, the elastic wave propagates in the direction of the load axis and if $c=0$, it propagates in the direction perpendicular to the load axis. The effective Vp can be evaluated as a function of differential stress by equations (3.2.13), (3.2.14) and (3.2.3) to (3.2.5). The last three equations (3.2.3) to (3.2.5) can be used to calculate the deformation of the cracks due to differential stress. In the calculation of the effective Vp by a computer, we consider that cracks with sufficiently small aspect ratios, say less than 10^{-8}, are closed completely.

(iv) Theoretical Calculation for Anisotropic Vp Change in the Stage of Compaction Under Uniaxial Compression

We calculate the compressional wave velocities with respect to differential stress and compare the calculated Vp with the measured one. We investigate the case of uniaxial compression. The calculated Vp's and DV/V's are plotted against differential stress in Fig. 29 for CGM and in Fig. 30 for FGM, in which the measured ones are also plotted. We first calculate the Vp's and the DV/V's in terms of ϕ^0, K, G, ρ and the DSC's obtained in section 3.1-(iv) (case A in these figures). The calculated values are in poor agreement with the measured ones. Next we calculate the Vp's and the DV/V's, taking account of the effect of tensile-shear crack interaction which is mentioned later, and as a trial we adjust the initial total porosity ϕ^0 (case B in these figures), which, however, is not the reasonable parameter. In most studies except those by Toksöz et al. (1976) and Cheng and Toksöz (1979), ϕ^0 has been treated as an adjustable parameter. Therefore it is considered that those results are unreasonable. In case B, the calculated Vp's and DV/V's are almost in agreement with the measured ones. However, this result is also unreasonable.

In order to interpret the deviation between the calculated and measured

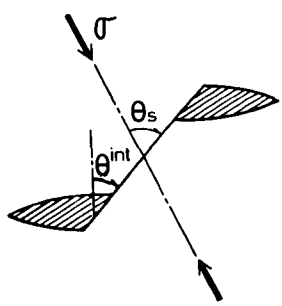

Fig. 31 A model of tensile-shear crack interaction. Crack geometry associated with the applied stress field are shown. The effect of friction on the sliding of shear cracks are taken into account. See the text for details.

values for case A, we make the following calculations taking account of four effects of cracks on Vp : tensile-tensile crack interaction (cane C), tensile-shear crack interaction (case D), isolated shear cracks (case E), and, deformation of a crackin an anisotropic medium (case F).

Case C : Tensile-tensile crack interaction

The analytical consideration of 3-dimensional tensile-tensile crack interaction has not been made. Therefore the effect of the interaction on Vp can not exactly be taken into account in the calculation of the effective compressional wave velocity. However, it is inferred from the analytical solution for 2-dimensional tensile-tensile crack interaction (e.g., Sneddon and Lowengrub, 1969) that the cracks interacting with each other are deformed more easily than the isolated cracks under the same stress, in other words, they see the soft medium rather than the crack-free medium. Thus the effect of tensile-tensile crack interaction is approximately taken into account by calculating the deformation of cracks using the effective elastic constants.

Case D : Tensile-shear crack interaction

The interacting crack model as shown in Fig. 31 has been proposed to explain a hysteresis of dilatancy for a rock by Scholz and Kranz (1974), Stevens and Holcomb (1980) and Moss and Gupta (1982). The interacting cracks have been observed using SEM (scanning electron microscope) by Batzle et al. (1980). If there are such types of cracks in the rocks, then tensile cracks connecting with shear cracks may be deformed more easily than isolated tensile cracks. The surface displacement of a tensile crack depends on the angle (θ^{int}) between a tensile crack and a shear crack (Fig. 31), the frictional coefficient on the surface of the shear crack, and the stress condition. Let a shear crack make an angle of θ_s to the load axis. If the condition that θ_s is less than $\theta_\mu = \tan^{-1}\frac{1}{\mu}$ (μ is the frictional coefficient) is satisfied, shear cracks will slide. We take account of the effect of the tensile-shear crack interaction by adding the deformation of tensile cracks due to the sliding of shear cracks, if the sliding condition is satisfied. This additional surface displacement of a tensile crack Δu may be approximately given as $\Delta u = u \cos\theta^{int}$, where u is the surface displacement of an isolated tensile crack given by equation (3.2.3).

Case E : Isolated shear cracks

We take account of the effect of isolated shear cracks. Some tensile cracks close completely by applied compressive stress. Even after closing, these cracks affect the effective elastic constants under shear stress. Therefore, we regard a closed tensile crack as a shear crack. Since the effective bulk

modulus of a medium containing shear cracks is equal to the crack-free bulk modulus (Jaeger and Cook, 1971), only the elastic constants associated with shear modulus are affected by the shear cracks.

Case F : Deformation of a crack in an anisotropic medium

The deformation of a crack in an isotropic medium has been derived in section 3.2-(ii). Therefore we need to correct that deformation, if the deformation of a crack occurs in the anisotropic medium. In general, the stress-strain relations in an isotropic medium under uniaxial stress are

$$\varepsilon_{axial}=\frac{\sigma}{E}, \qquad \varepsilon_{lateral}=-\frac{\nu}{E}\sigma, \tag{3.2.15}$$

where ε_{axial} and $\varepsilon_{lateral}$ are strains parallel to and perpendicular to the load axis, respectively, σ the uniasial stress, and E and ν the Young's modulus and the Poisson's ratio of an isotropic medium. On the other hand, the stress-strain relations in an anisotropic medium with the axial symmetry are

$$\hat{\varepsilon}_{axial}=\frac{\sigma}{\hat{E}}, \quad \hat{\varepsilon}_{lateral}=-\frac{\hat{\nu}}{\hat{E}}, \tag{3.2.16}$$

where

$$\frac{1}{\hat{E}}=\frac{C_{11}^{*}+C_{12}^{*}}{C_{33}^{*}(C_{11}^{*}+C_{12}^{*})-2C_{13}^{*2}}, \qquad \hat{\nu}=\frac{C_{13}^{*}}{C_{11}^{*}+C_{12}^{*}}.$$

and C_{ij}^{*} is the effective elastic constants defined in the X-system (see Fig. 28).

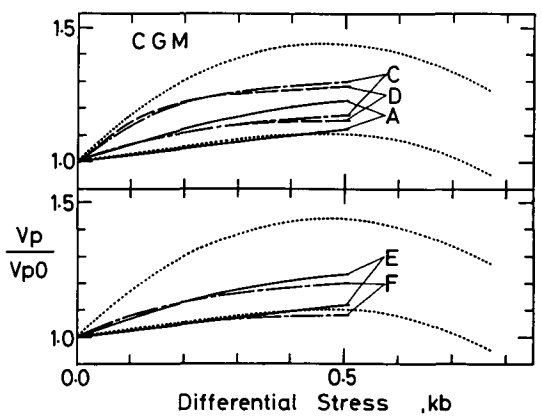

Fig. 32 Theoretical estimations of the effects of tensile crack interaction, tensile-shear crack interaction, isolated shear cracks and deformation of a crack in an anisotropic medium on Vp for CGM. A : calculated Vp change based on the DSC, C, D, E and F : calculated Vp changes by taking account of the effects of tensile-tensile crack interaction, tensile-shear crack interaction, isolated shear cracks and deformation of a crack in an anisotropic medium, respectively. These single effects could not improve the result.

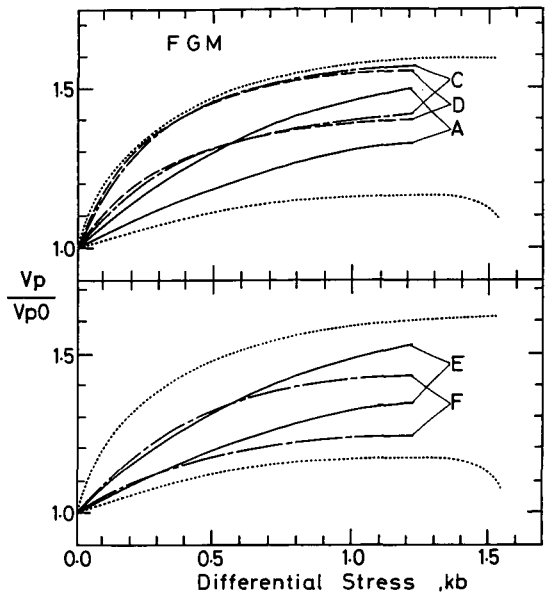

Fig. 33 Same as in Fig. 32 for FGM.

In general, the strains in a direction making an angle of θ with the load axis and in a direction perpendicular to that axis are

$$\left.\begin{aligned} \varepsilon_\theta &= \varepsilon_{axial}\cos^2\theta + \varepsilon_{lateral}\sin^2\theta, \\ \varepsilon_\theta^\perp &= \varepsilon_{axial}\sin^2\theta + \varepsilon_{lateral}\cos^2\theta. \end{aligned}\right\} \tag{3.2.17}$$

Thus if an OS crack whose normal makes an angle of θ with the load axis is deformed under uniaxial stress in an anisotropic medium, the expressions for the strains of an isotropic medium, ε_θ and $\varepsilon_\theta^\perp$, are replaced by the following approximate formula:

$$\left.\begin{aligned} \frac{\hat{\varepsilon}_\theta}{\varepsilon_\theta} &= \frac{1-(1+\hat{\nu})\sin^2\theta}{1-(1+\nu)\sin^2\theta}\frac{E}{\hat{E}}, \\ \frac{\hat{\varepsilon}_\theta^\perp}{\varepsilon_\theta^\perp} &= \frac{\hat{\nu}-(1+\hat{\nu})\sin^2\theta}{\nu-(1+\nu)\sin^2\theta}\frac{E}{\hat{E}}, \end{aligned}\right\} \tag{3.2.18}$$

where $\hat{\varepsilon}_\theta$ and $\hat{\varepsilon}_\theta^\perp$ are the strains of an anisotropic medium. If these strains correspond to the strains at the directions of a short axis and a long axis of a crack, the deformation of a crack in an anisotropic medium can be expressed by using equations (3.2.3) and (3.2.18). The elastic moduli E and ν for an isotropic medium are given as the averaged values of Voigt and Reuss averages (e.g., Simmons and Wang, 1971).

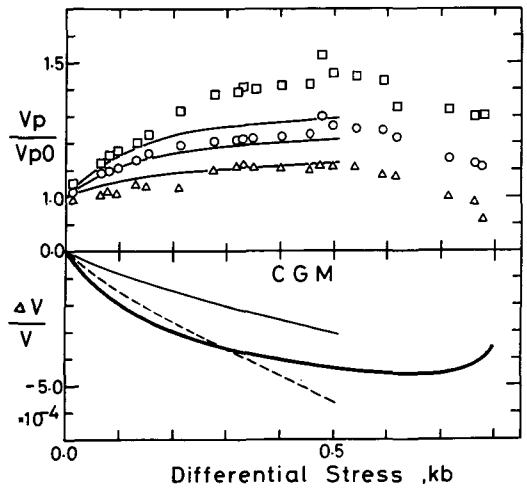

Fig. 34 Calculated Vp and strain changes due to differential stress, by taking account of all the effects of cracks, in the stage of compaction for CGM (thin solids lines). If the elastic moduli reduces by the sliding of shear cracks, a volumetric strain change drawn by a broken line is obtained. Note that this result on anisotropic Vp change is improved in comparison with the calculated result based on the DSC (A in Fig. 32).

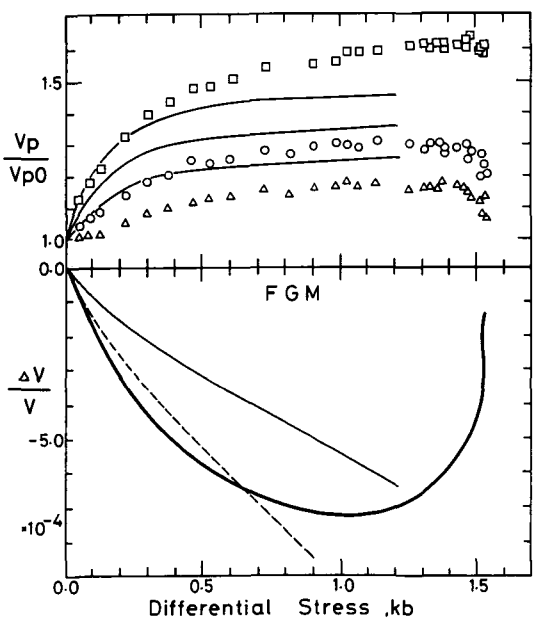

Fig. 35 Same as in Fig. 34 for FGM. Note that this result is improved in comparison with the calculated result based on the DSC (A in Fig. 33).

The calculated Vp curves designated by A, C, D, E and F shown in Fig. 32 for CGM and Fig. 33 for FGM correspond to the cases A, C, D, E and F. Comparing these cases with the case A, we see the following: for two kinds of crack interactions Va increases at low differential stress; for the isolated shear cracks Vp decreases and the normarized Vp or Va do not change; and, the anisotropy of the medium has a little effect on Va.

Single effect of cracks could not improve the result. We proceed to calculate taking account of all the effects from case C to case F. In this calculation, the number of preexisting shear cracks and θ^{int} were determined by trial and error. The calculated Vp's and DV/V's are shown in Fig. 34 for CGM and in Fig. 35 for FGM, in which the measured ones are also shown. For CGM, the calculated Vp is in good agreement with the measured one except for Vp'' (Fig. 34). For FGM, the calculated Vp'' agrees with the measured one at lower differential stress (Fig. 35). The complete agreement between the calculated and measured Vp's is not obtained in the range of compaction, but the disagreement between both Vp's is improved to some extent, that is not, however, for the single effect. The fact that VA due to compaction by a uniaxial compression is not sufficiently explained by the theory may be due to the difference in boundary conditions; in the experiment, rock samples have a free boundary while the theory employs an infinite medium for the deformation of a crack.

In addition, we calculate the volumetric strain using equation (3.2.16) according to the same procedure as that in section 3.1-(iii). We consider a case in which the slidings of shear cracks lower the elastic moduli from dynamic ones to static ones. The measured and two calculated volumetric strains are shown as a function of differential stress in Fig. 34 for CGM and in Fig. 35 for FGM. One of the calculated volumetric strains (thin solid lines) is obtained from the dynamic moduli which have been given in the calculation of Vp. The other one is calculated in terms of the lowered moduli (broken lines). These calculations do not improve the resultant volumetric strains. If the ratios of static Young's modulus to a dynamic one are assumed to be 0.44 for CGM and 0.47 for FGM, the calculated volumetric strains can be fitted to the measured ones within the experimental error as shown by the broken lines in Fig. 34 and Fig. 35. It is of no use to continue to calculate at differential stress higher than p'_d where dilatancy occurs, because the disagreement at lower differential stress mentioned above increases at higher differential stress.

(v) Theoretical Calculation for Anisotropic Vp Change Under Triaxial Stress Conditions

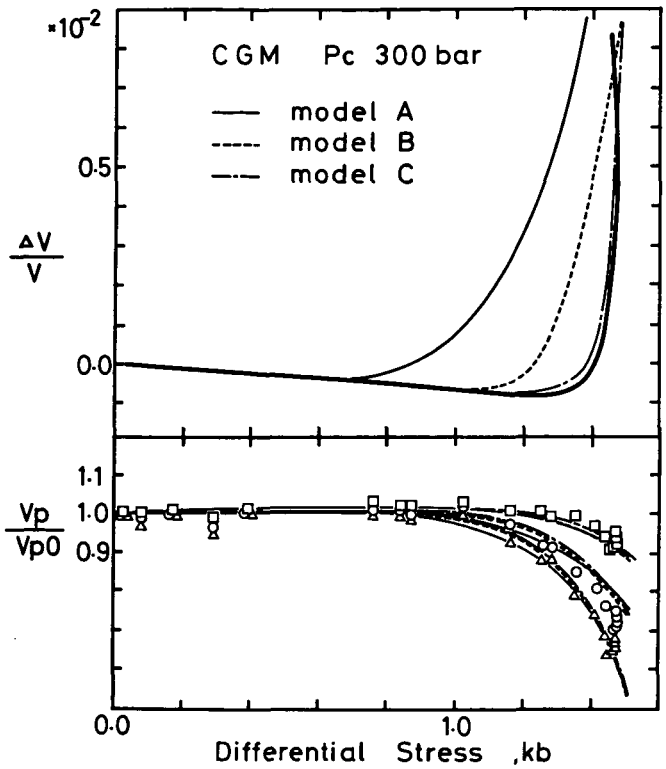

Fig. 36 Calculated Vp and strain changes and measured Vp and strain changes in the whole process from compaction to dilatancy at Pc=300 bars for CGM. Calculations in the stage of dilatancy were made for three models on the process of the occurrence of dilatant cracks (model A : aspect ratios of dilatant cracks are constant during dilatancy, model B : those change suddenly at a certain differential stress, model C : those change continuously during dilatancy). Note that the measured Vp and strain changes are explained well by model C.

In this section, we will examine the results of the theoretical calculation of Vp, and note, especially, the relationship between VA and dilatancy. We examine the feature of the occurrence of cracks. We call the cracks generated in a rock 'dilatant cracks'. It is inferred from the number of AE (acoustic emission) detected that the number of dilatant cracks per unit of stress increases exponentially with increasing differential stress (e.g., Mogi, 1962 ; Scholz, 1968 b). Therefore we assume that the number of dilatant cracks is an exponential function of differential stress ; that is, of the form $a(e^{b\sigma}-1)$, and by trial and error we look for proper values of a and b in such a manner that the changes of Vp and of DV/V, as a function of differential stress, will be explained

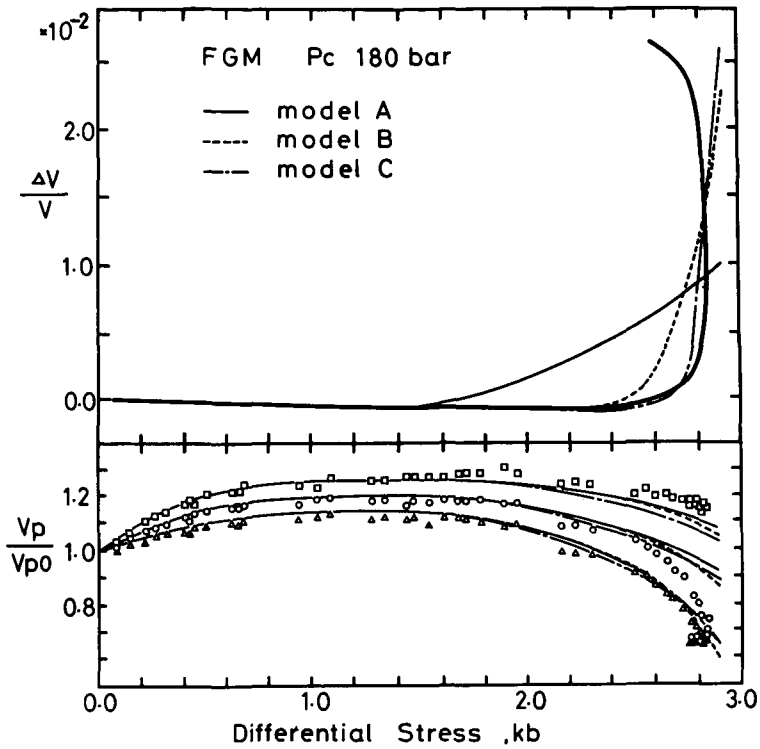

Fig. 37 Same as in Fig. 36 at Pc=180 bars for FGM. Calculated result in the stage of compaction, by taking account of the effect of tensile-shear crack interaction and the initial Va, agrees well with the measured one.

quantitatively.

The observations of dilatant cracks were made recently by using SEM (Sprunt and Brace, 1974; Tapponnier and Brace, 1974; Hadley, 1976; Olsson and Peng, 1976). These observations showed that the dilatant cracks whose normals are almost perpendicular to the load direction were dominant, and that the aspect ratios of these cracks were in the range of $10^{-2}-10^{-4}$. Taking these observations into account, we assume that the directional dependence of the number of dilatant cracks at a given differential stress is given as a function of $\cos^2\theta$, where θ is the angle between the crack orientation and the load direction.

The calculated Vp's and DV/V's at $Pc=300$ bars for CGM and at $Pc=180$ bars for FGM are shown in Fig. 36 for CGM and in Fig. 37 for FGM, in which the measured ones are also shown. The calculated Vp and DV/V are identical in the stage of compaction. For CGM, since most pre-existing cracks are

closed by the applied confining pressure, the calculated results in the stage of compaction agree very well with the measured ones even if any effects of cracks mentioned in section 3.2-(iv) are not taken into account. For FGM, taking account of the initial Va (about 3%) and tensile-shear crack interaction ($\theta^{int}=40°$), the calculated results in the stage of compaction agree well with the measured ones. Since it is considered that there remain many pre-existing cracks in a FGM sample under applied confining pressure, the effect of tensile-shear crack interaction should be taken into account on the calculation of Vp for FGM.

We discuss the results obtained in the stage of dilatancy. We examined three cases for the process of the occurrence of dilatant cracks. In case A, we calculated Vp and DV/V assuming that the aspect ratios of dilatant cracks are constant with increasing differential stress. If the calculation is made so as to fit the measured Vp data rather than the strain data, assuming that the constant aspect ratio equals 0.1, then the calculated strain curves do not agree with the measured ones at all as shown in Fig. 36 for CGM and in Fig. 37 for FGM. The change in the value of aspect ratio does not affect the result, because the change is compensated by the change of the number of dilatant cracks. In case B, we calculated Vp and DV/V assuming that the aspect ratio of dilatant cracks change suddenly at a differential stress of 1300 bars for CGM and at a differential stress of 2500 bars for FGM. Although the calculated Vp curves fit the measured Vp data well, even in case B, the calculated strain curves do not agree very well with the measured ones. In case C, we calculated Vp and DV/V assuming that the aspect ratio of dilatant cracks change continuously with increasing differential stress. In this case, the calculated curves for Vp and those for DV/V agree well with the measured ones. For CGM, when an initial aspect ratio of dilatant cracks is assumed to be 10^{-4} to 4×10^{-4}, the parameters a and b are obtained to be 2.0 and 0.0042/bar. For FGM, when an initial aspect ratio of dilatant cracks is assumed to be 10^{-4} to 4×10^{-4}, the parameters a and b are obtained to be 5.5 and 0.002/bar. We conclude that, under confining pressure, all the anisotropic variation of Vp and the change of volumetric strain with differential stress can be explained quantitatively by OS cracks.

However, Figure 36 and Figure 37 show that there exists a discrepancy between the calculated and measured Vp for a direction of 45° over a differential stress. The differential stress is about 1400 bars for CGM and about 2600 bars for FGM. It is known that there is a marked clustering of microfractures on the final fault plane of a rock (e.g., Mogi, 1968 ; Scholz, 1968 a ; Nishizawa et al., 1981). Since it has been observed that the final fault plane in formed on the

Table 3 List of initial Vp

No.	initial Vp (km/sec)
CGM-1	4.88 (1.00)
CGM-2	6.05 (1.24)
CGM-3	6.39 (1.31)
CGM-4	6.44 (1.32)
CGM-5	6.49 (1.33)
FGM-1	4.08 (1.00)
FGM-2	5.59 (1.37)
FGM-3	6.61 (1.62)
FGM-4	6.69 (1.64)
FGM-5	7.02 (1.72)

The initial Vp is the Vp at a differential stress of zero.

plane inclined at an angle lower than 45° to the load direction (e.g., Jaegar and Cook, 1971), the measured Vp in a direction oblique to the load axis is considered to become lower than a value expected from a uniform occurrence of dilatant cracks.

3.3 Relation Between Va^{max} and Initial Vp

We derive a simple relation between Va due to compaction and the increase of an initial Vp. The experiments suggest that there are two kinds of phenomena relating to pre-existing cracks: Vp increases by confining pressure; and, VA becomes excessive in a rock with increasing differential stress. Both phenomena can be explained by the closing of pre-existing cracks. Figure 24 shows that Va^{max} decreases exponentially with increasing confining pressure, while the initial Vp increases with increasing confining pressure as listed in Table 3. These initial Vp's are a little larger than those expected from the Vp changes measured under confining pressure (see Fig. 4 and Fig. 5), because the samples used to measure the initial Vp were at a confining pressure for a longer time than those used to measure Vp shown in Fig. 4 and Fig. 5. Figure 38 shows the relation between Va^{max} and the increase of the initial Vp.

We try to derive the relation theoretically. Since Vp is greatly affected by the cracks with an aspect ratio less than 10^{-3}, the model of penny-shaped cracks instead of that of the OS cracks is employed for simplicity. Let the effective elastic constants associated with Vp be $C_{11}^*(=C_{22}^*)$ and C_{33}^*, which are obtained by using equation (3.2.13).

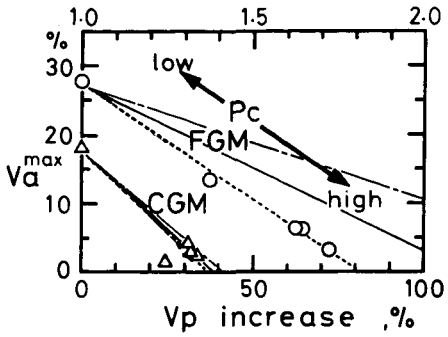

Fig. 38 Observed and theoretical relations between the maximum Va due to compaction and the increase of initial Vp. The linear relationship was obtained both for observation and for theory. The slopes of theoretical relations were calculated by two kinds of initial crack densities which were obtained from the Va^{max} and from the increase of initial Vp, respectively. The relations with those slopes for the former initial crack density and for the latter one are shown by dott-dash-lines and solid lines, respectively.

The effect of crack closure, that is, the variation of crack porosity, is expressed with a parameter, a, as

$$\phi(a,\ \theta,\ \psi)=\frac{4}{3}\pi a\varepsilon\left(1-\frac{a}{2}-\frac{a}{2}\cos 2\theta\right), \tag{3.3.1}$$

where $\phi(a,\ \theta,\ \psi)$ is the crack porosity with aspect ratio a in the direction θ, ψ, ε the crack density, and 'a' the parameter of crack closure. The derivation of this equation is given in appendix C. Because 'a' is defined as the normalized differential stress, $a=0$ prescribes the state of zero stress, and $a=1$ prescribes the state of closure stress of cracks whose normals coincide with the load axis. When $a=0$, the crack porosity is independent of θ and ψ; that is, the distribution of the directions of crack normals is isotropic. When $a\neq 0$, the crack porosity depends on θ; that is, the distribution of the directions of crack normals is anisotropic with respect to θ. For $a=1$, the porosity of cracks whose normals coincide with the load axis becomes zero, and the porosity of cracks whose normals are perpendicular to the load axis is unchanged.

The expression for the effective elastic constants given in equation (3.2.13) is rewritten using equation (3.3.1) in the following form,

$$C^{*}_{ijkl}=C_{ijkl}-\sum_{n=1}^{N}\int_{0}^{2\pi}d\psi\int_{0}^{\pi}\phi(a_n,\ \theta,\ \psi)\hat{C}_{ijkl}(a_n,\ \theta,\ \psi)\sin\theta d\theta, \tag{3.3.2}$$

where

$$\hat{C}_{ijkl}(a_n,\ \theta,\ \psi)=C_{ijpq}A_{pqkl}(a_n,\ \theta,\ \psi). \tag{3.3.3}$$

The effective elastic constants associated with Vp are now expressed by using

equation (3.3.2),

$$C_{11}^{*}=C_{1111}^{*}=\left(K+\frac{4}{3}G\right)-\sum_{n=1}^{N}\int_{0}^{2\pi}d\psi\int_{0}^{\pi}\phi(\alpha_n,\ \theta,\ \psi)\hat{C}_{1111}(\alpha_n,\ \theta,\ \psi)\sin\theta d\theta,$$

$$C_{33}^{*}=C_{3333}^{*}=\left(K+\frac{4}{3}G\right)-\sum_{n=1}^{N}\int_{0}^{2\pi}d\psi\int_{0}^{\pi}\phi(\alpha_n,\ \theta,\ \psi)\hat{C}_{3333}(\alpha_n,\ \theta,\ \psi)\sin\theta d\theta, \tag{3.3.4}$$

where

$$\hat{C}_{1111}(\alpha_n,\ \theta,\ \psi)=\left(\tilde{C}_{1111}\cos^4\theta+\tilde{C}_{3333}\sin^4\theta+\frac{\tilde{C}_{1133}}{2}\sin^2 2\theta+\tilde{C}_{2323}\cdot\right.$$
$$\left.\cdot\sin^2 2\theta\right)\cos^4\psi+\tilde{C}_{1111}\sin^4\psi+\frac{1}{2}(\tilde{C}_{1133}\sin^2\theta+\tilde{C}_{1122}\cdot$$
$$\cdot\cos^2\theta)\sin^2 2\psi+\left(\frac{\tilde{C}_{1111}-\tilde{C}_{1122}}{2}\cos^2\theta+\tilde{C}_{2323}\sin^2\theta\right)\cdot$$
$$\cdot\sin^2 2\psi,$$

$$\hat{C}_{3333}(\alpha_n,\ \theta,\ \psi)=\tilde{C}_{1111}\sin^4\theta+\tilde{C}_{3333}\cos^4\theta+\frac{\tilde{C}_{1133}}{2}\sin^2 2\theta+\tilde{C}_{2323}\sin^2 2\theta.$$

Here C_{ijkl} is a function of K, G and α_n. The explicit forms of C_{ijkl} are given in appendix D. Substituting the explicit expressions for C_{ijkl} into equation (3.3.4) and integrating them with respect to θ and ψ, we have after some manipulations,

$$\left.\begin{aligned}C_{11}^{*}&=\left(K+\frac{4}{3}G\right)\left[1-\frac{4}{45}\varepsilon^{*}\left\{\left(1-\frac{a}{2}\right)f(R)+\frac{a}{2}g(R)\right\}\right],\\ C_{33}^{*}&=\left(K+\frac{4}{3}G\right)\left[1-\frac{4}{45}\varepsilon^{*}\left\{\left(1-\frac{a}{2}\right)f(R)+\frac{a}{2}h(R)\right\}\right],\end{aligned}\right\} \tag{3.3.5}$$

where

$$\left.\begin{aligned}f(R)&=\frac{45-150R+208R^2-96R^3}{R(1-R)(3-2R)},\\ g(R)&=\frac{105-238R+304R^2-160R^3}{7R(1-R)(3-2R)},\\ h(R)&=\frac{105-574R+848R^2-352R^3}{7R(1-R)(3-2R)},\end{aligned}\right\} \tag{3.3.6}$$

Here $\varepsilon^{*}(=4\pi\sum_{n=1}^{N}\varepsilon_n)$ is the total crack density and R is constant determined by the crack-free elastic moduli as given in appendix D.

According to the definition of Va given in equation (3.2.1), we have the approximated Va in the first order;

$$Va=\frac{\frac{1}{45}a\varepsilon^{*}\{g(R)-h(R)\}}{1-\frac{2}{45}\varepsilon^{*}\left\{\left(1-\frac{a}{2}\right)f(R)+\frac{a}{2}\frac{g(R)+h(R)}{2}\right\}}. \tag{3.3.7}$$

Setting $a=0$, Va is zero because of no differential stress. Let ε_0^{*} be the crack

Table 4 List of slopes of the relation between Va^{max} and initial Vp increase

	K(Mb)	G(Mb)	γ(a=1)	γ'(a=1)	γ(a=2)	γ'(a=2)	γ(a=2.5)	γ'(a=2.5)	γ(observed)
CGM	0.75	0.346	0.25	0.25	0.37	0.40	0.43	0.46	0.49
FGM	1.048	0.311	0.13	0.17	0.15	0.23	0.16	0.24	0.35

γ, γ' : slopes of the relation calculated by using initial crack densities which are obtained from the Va^{max} and from the increase of initial Vp, respectively.
a : normalized differential stress (see Appendix C)

density in a rock at $Pc=0$, and ε_1^* the crack density at $Pc=P$. Assuming that $\varepsilon_1^*=\varepsilon_0^*-\Delta\varepsilon(\Delta\varepsilon>0)$, Va for $\varepsilon^*=\varepsilon_1^*$ are approximately represented by using Va for $\varepsilon^*=\varepsilon_0^*$ as follows:

$$Va(\varepsilon_1^*)=Va(\varepsilon_0^*)-\frac{\frac{1}{45}aB(R)\Delta\varepsilon}{\left\{1-\frac{2}{45}\varepsilon_0^*A(a,\ R)\right\}^2}, \tag{3.3.8}$$

where

$$A(a,\ R)=\left(1-\frac{a}{2}\right)f(R)+\frac{a}{2}\frac{g(R)+h(R)}{2},$$
$$B(R)=g(R)-h(R).$$

In the same way, the change of the initial Vp due to the change of crack density is given by using equation (3.3.5), in which the parameter 'a' is assumed to be zero. Neglecting the change of effective density due to the change of crack density because its effect on Vp is the second order, we have the relative Vp change (ΔVp) as

$$\Delta Vp(\varepsilon_1^*)\left(\equiv\frac{Vp(\varepsilon_1^*)-Vp(\varepsilon_0^*)}{Vp(\varepsilon_0^*)}\right)=\frac{\frac{2}{45}f(R)\Delta\varepsilon}{1-\frac{2}{45}\varepsilon_0^*f(R)}. \tag{3.3.9}$$

Comparing equation (3.3.8) with equation (3.3.9), we obtain the following relation Va and ΔVp :

$$Va(\varepsilon_1^*)=Va(\varepsilon_0^*)-\gamma\Delta Vp(\varepsilon_1^*), \tag{3.3.10}$$

where

$$\gamma=\frac{a}{2}\frac{B(R)}{f(R)}\frac{1-\frac{2}{45}\varepsilon_0^*f(R)}{\left\{1-\frac{2}{45}\varepsilon_0^*A(a,\ R)\right\}^2}. \tag{3.3.11}$$

The linear relationship between Va and ΔVp with a negative slope ($-\gamma$) has been proved. It is clear that the γ is a function of an initial crack density and the crack-free elastic moduli. Since the initial crack density can be given in two ways (from equation (3.3.7) and from equation (3.3.9)), two kinds of slopes (say, γ and γ') were calculated. Since there is no way of prescribing the

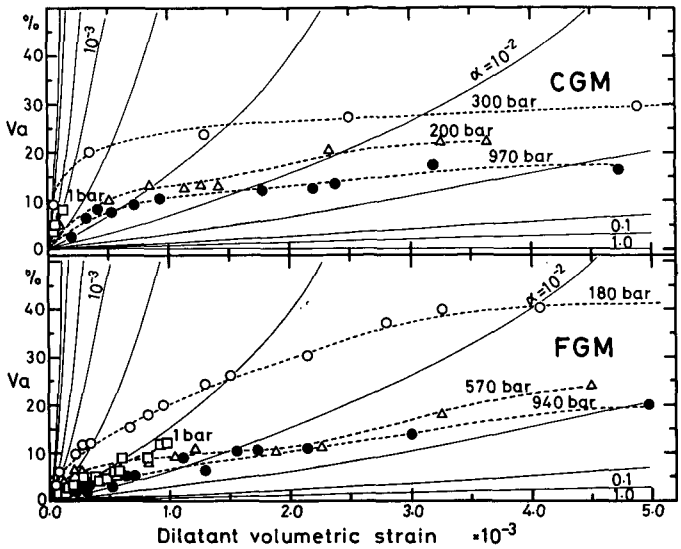

Fig. 39 Observed and theoretical relations between Va due to dilatancy and dilatant volumetric strain. Theoretical curves calculated assuming that aspect ratios of cracks are constant are drawn by solid thin lines. Note that a smoothed curve through the measured values for each confining pressure is intersected by those theoretical curves.

parameter 'a' necessary for obtaining Va^{max}, we tried to calculate the slopes for three cases $a=1$, $a=2$ and $a=2.5$. These calculated values of γ and γ' are listed in Table 4. If $a=2.5$, the calculated relations agree with the measured ones within the errors of 5% for CGM and 30% for FGM. The condition for $a=2.5$ corresponds to the one where all the cracks, which have the normals making an angle of at most 50° with the load axis, are closed.

3.4 Shapes of Dilatant Cracks and Physical Process of Dilatancy

We will investigate here the physical process of dilatandy experimentally as well as theoretically. We examine a relation between Va due to dilatancy and the dilatant volumetric strain for each rock. The relation obtained from the experiments is shown in Fig. 39. Since a shape of the crack generated during dilatancy has not been known, we calculate the Va for dilatant volumetric strain with a value of the aspect ratio assumed. Calculated Va increases exponentially with increasing dilatant volumetric strain. These calculated values for different values of aspect ratio are also shown in Fig. 39. Clearly, a smoothed curve through the measured values for each confining pressure is intersected by the calculated curves.

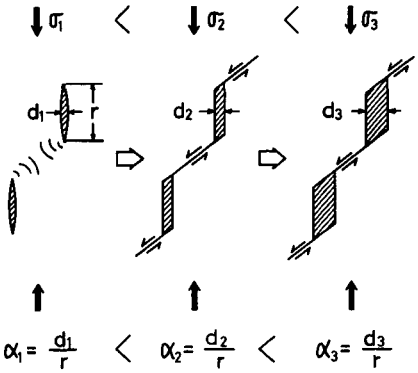

Fig. 40 A qualitative model for the growing process of aspect ratios of dilatant cracks. The growing process of aspect ratios can be described as follows: dilatant cracks with small aspect ratio (e.g., α_1) are generated one after another. These cracks begin to interact with each other at a differential stress and finally those are interconnected through a shear crack. Aspect ratio of these interconnected cracks begin to grow due to the sliding of shear cracks. If such a process is continued during dilatancy, aspect ratios of dilatant cracks may be continued to grow.

These intersections explain the change of the shape of cracks in the stage of dilatancy; that is, dilatant cracks with an aspect ratio of $O(10^{-4})$ are generated in the early stage of dilatancy. The flatter the shape of a crack, the more it effects VA. Therefore, VA due to dilatancy increases rapidly even for a small change of dilatant volume. As the dilatancy advances from its middle stage to the final stage, the shapes of dilatant cracks change continuously from very flat ones ($\alpha \simeq 10^{-4}$) to thicker ones ($\alpha \simeq 10^{-1} - 10^{-2}$) with increasing dilatant volumetric strain. We have already used this result on the shapes of dilatant cracks to calculate the Vp and DV/V in section 3.2-(V).

We will consider the mechanism by which the aspect ratio of a dilatant crack grows. Theoretical calculation only indicates that thickened cracks must dominate at an advanced stage of dilatancy. However, whether such cracks are created originally or grow up from the thinner ones is not certain. The former explanation is unreasonable judging from the observations of cracks by SEM (Brace et al., 1972; Sprunt and Brace, 1974; Tapponnier and Brace, 1974; Hadley, 1976; Olsson and Peng, 1976; Tapponnier and Brace, 1976; Kranz, 1979; Batzle et al., 1980). Kranz (1979) has observed that cracks distributed side by side interacted with each other. His case is that two tensile cracks are interconnected through a shear crack. If this is also true for our experiments, we can expect the growth of the aspect rations of cracks during

the advance of dilatancy by the mechanism shown in Fig. 40. The calculated results in Fig. 39 show that the thicker cracks are less effective in making Va increase than the thinner ones which have the same porosity. According to this result, we conclude that the gradual decrease of the Va changing rate with volumetric strain (see section 3.2-(i)) is due to the growth of the aspect ratios of dilatant cracks. This may be modeled as shown in Fig. 40.

4. Discussion

In this chapter, we will briefly discuss problems arising from the theoretical considerations and also describe the application of the results obtained in chapter 3.

We will discuss the reason why the anisotropic Vp change measured under uniaxial stress could not sufficiently be explained by the OS crack model based on Eshelby's theory. Theoretical considerations on the results obtained under triaxial stress show that the difference between the calculated and measured Vp decreases with increasing confining pressure, through the process of compaction. Since the difference between those under a uniaxial stress is not satisfactorily improved even by taking the effect of crack interaction into account, it is considered to be caused by the difference in boundary condition ; that is, in the experiment, the rock samples have a free surface, while the theory assumes an infinite medium for the deformation of a crack. We consider an imaginary sample in an infinite medium. The imaginary sample has the same shape as a rock sample. For a uniaxial stress, the stress-free condition is satisfied on the side boundary of a rock sample. On the other hand the stress-free condition is not satisfied on the side boundary of the imaginary sample. A normal stress required to constrain a displacement and a secondary stress field due to the deformation of cracks are applied on the side boundary of the imaginary sample. Therefore, a discrepancy between the experimental results and theoretical ones arises. For a triaxial stress, the rock sample as well as the imaginary sample are subjected to confining pressure. In addition, the normal stress and the secondary stress field are applied on the side boundary of the imaginary sample. Therefore, even in this case, a discrepancy between the experimental results and theoretical ones arises. The magnitude of the secondary stress field get smaller as cracks are closed by the application of confining pressure. Futhermore, since the normal stress, which is required to constrain a displacement on the imaginary boundary, is independent of confining pressure, the effect of the normal stress on a velocity change becomes less relatively as confining pressure

increases. Consequently the confining pressure being applied to the rock sample, the discrepancy between the boundary condition in the experiment and the theory is reduced, and so the anisotropic Vp change measured under triaxial stress is well explained by the oblate spheroidal crack model.

Theoretical considerations show that Va^{max} decreases linearly as the initial Vp increase becomes larger. The theoretical considerations are based on Eshelby's theory, but are made by using a penny-shaped crack model in place of the OS crack model. Theoretical calculations also indicate that the slope of the relation (between Va^{max} and the initial Vp increase) derived by the theory coincides with that measured for CGM within the error of 5% and for FGM within the error of 30%, but both the slopes given by the theoretical relation and the experimental one are slightly different for both rocks. The initial Vp increase is well explained by the OS crack model (section 3.1-(vi)), but the Va^{max} in the case of a uniaxial stress is not sufficiently explained by the OS crack model (section 3.2-(vi)). In addition, if a crack density of a pennyshaped crack for each aspect ratio is given so as to satisfy the DSC determined by using the OS crack model, the calculated results by the penny-shaped crack model almost agree with those by the OS crack model. Therefore, if a theoretical relation between the initial Vp increase and Va^{max} is derived by using the penny-shaped crack model, the relation may not closely agree with the experimental relation.

Theoretical considerations on the physical process of dilatancy were made by assuming that cracks in a rock do not interact with each other. However, if the increase of aspect ratios of dilatant cracks occurs in a rock, cracks in a rock will interact with each other. Therefore, we will briefly discuss how crack interaction affects the physical process of dilatancy. Supposing the crack porosity is constant, the effect of a crack on the effective elastic moduli in an interacting condition is larger than that in a non-interacting condition. When the aspect rations of interacting cracks are equal to those of noninteracting ones, the anisotropic Vp changes on dilatancy will be explained by fewer interacting cracks than noninteracting cracks. Therefore, the parameters 'a' and 'b' (see page 45) on the number of the occurrence of dilatant cracks may be overestimated to some extent.

Comparison of the results for two kinds of rocks shows that Va due to compaction for FGM is larger than that for CGM. The most effective factor on the Va is the distribution of aspect rations of cracks. The elastic parameters of minerals in rocks affect also the Va. Equation (3.3.7) shows that the Va changes with the crack-free elastic moduli of a medium so that the Va may increase as the Poisson's ratio of a medium increases. Since the Poisson's ratio

is 0.3 for CGM and 0.365 for FGM, the Va in the FGM must be larger than that in the CGM; this explains the experimental fact stated above.

We will consider the application of the results on Vp measured. The effect of water on VA should be taken into account in order to apply our data in field measurements. Although the effect of water on VA is not clear experimentally, this can be estimated from the effect of water on Vp (e.g., Nur and Simmons, 1969b). When water permeates into a rock, Vp increases. If there are cracks having the normals which are perpendicular to the propagation direction of compressional wave, the Vp does not decrease effectively by those cracks. If there are cracks having the normals which are parallel to its direction, the Vp decreases effectively by those cracks. Thus we will call the cracks of which the directions of nomals coincide with the propagation direction of compressional wave 'effective cracks'. When differential stress is applied to the rock, cracks of which the directions of normals coincide with the load direction are closed selectively. Therefore the distribution of effective cracks becomes anisotropic. The more the effective crack porosity increases, the larger the Vp increase by permeated water becomes. Since the effective crack porosity in the direction parallel to the load axis is small, Vp in that direction only slightly increases by permeated water. However, since the effective crack porosity in the direction perpendicular to the load axis is large, Vp in that direction increases markedly by permeated water. It is concluded that water makes Va decrease. The Va change due to differential stress depends on the experimental conditions on water which are classified as follows; one is a drained condition and the other is an undrained condition. The Va decrease by permeated water for the drained condition is expected to be less than that for the undrained condition. In addition, if there are tensile cracks interconnected through a shear crack in a rock, water affects not only Va but also the way of the Va change with differential stress, because of reduction of a frictional coefficient between shear crack surfaces. The rate of Va change for saturated or partially saturated rocks may become larger than that for dry rocks at low differential stress.

We will briefly describe the method of determining in-situ stress by using the anisotropic Vp change. The measurement of in-situ stress has been made by the hydraulic fracture method (e.g., Ikeda and Takahashi, 1981). This method is prominent one in measuring in-situ stress, but has difficulty because a large-scale measuring system is required. From the practical point of view, it is desirable to be able to measure in-situ stress easily by a simple device. If this can be done, an outbreake of an accident in coal mines may be prevented

by measuring in-situ stress by the simple device. Maeda and Shimizu (1983) devised a method of determining in-situ stress by using the Va due to differential stress and designed a simple device to measure Vp in twenty-eight directions. A principle of determining in-situ stress from the Vp's measured in many directions may be summarized as follows: the magnitude and direction of differential stress prescribe the state of the VA. When Vp's in many directions are measured under arbitrary triaxial stress, the values of Vp may be distributed on an ellipsoid. Since the Vp for the direction of maximum principal stress becomes the maximum Vp and the Vp for the direction of minimum principal stress becomes the minimum Vp, the directions of principal axes of the ellipsoid correspond to those of principal stress axes. Therefore, the directions of principal stresses can be easily determined. The magnitude of principal stresses can be estimated from the Vp increase or the Va. They confirmed the varidity of the principle by a room experiment and showed that the magnitude and direction of the maximum principal stress could be obtained with sufficient accuracy.

5. Summary of Conclusions

The following results may be drawn from the present study.

(1) For two kinds of calcareous rocks, the porosity distribution obtained from the Vp change due to confining pressure has one peak in the range of aspect ratio from 10^{-4} to 10^{-3}. The total crack porosity and the crack porosity occupied by cracks with aspect ratio more than about 4×10^{-4} for FGM is larger than those for CGM.

(2) The differential stress being applied to the rock, two kinds of VA; that is, VA by the closing of pre-existing cracks and VA by the generation of dilatant cracks, were observed under all the confining pressures measured.

(3) The former Va increases with increasing differential stress and reaches its maximum value before the occurrence of dilatancy. In this process, the average Vp is sure to increase.

(4) Maximum Va by the closing of cracks decreases exponentially with increasing confining pressure. The linear relation between this Va and the increase of the Vp at a differential stress of zero, with a negative slope, is derived from the experimental results as well as theoretical considerations.

(5) The latter Va increases exponentially with increasing differential stress. In this process, the average Vp is sure to decrease. In addition, the Va increases with increasing dilatant volumetric strain, but the change rate of the

Va decreases with increasing dilatant volumetric strain.

(6) The onest stress of dilatancy defined from the relation between Va and differential stress agrees well with that from the relation between volumetric strain and differential stress. The onset stress increases almost linearly with increasing confining pressure below 1 Kbars.

(7) The Vp and strain changes due to confining pressure are well explained quantitatively by the closing of the oblate spheroidal cracks based on Eshelby's theory.

(8) The anisotropic Vp and strain changes due to non-hydrostatic stress, for the whole process from compaction to dilatancy, are well explained quantitatively by using Eshelby's theory and taking account of the effect of crack interaction, except for the case of uniaxial compression.

(9) The crack interaction affects, more or less, the deformation of a rock under non-hydrostatic stress. The more the crack porosity increases, the more crack interaction comes to effect Vp change.

Acknowledgements

The auther wishes to express his deepest gratitude to Prof. Hiroshi Okada and Dr. Itaru Maeda for critical readings of the manuscript and helpful advises and suggestions. The author also wishes to thank Dr. Tsutomu Sasatani for his helpful advises. I thank Emeritus Prof. Kyozi Tazime and Dr. Takeo Moriya for their encouragements.

The numerical computations were carried out by HITAC M-200H at the Hokkaido University Computing Center.

This paper is the author's doctorial thesis submitted to the Hokkaido University in March, 1983.

References

Anderson, D.L., 1961. Elastic wave propagation in layered anisotropic media. J. Geophys. Res., **66**, 2953-2963.

Anderson, D.L., B. Minster and D. Cole, 1974. The effect of oriented cracks on seismic velocities. J. Geophys. Res., **79**, 4011-4015.

Batzle, M.L., G. Simmons and R.W. Siegfried, 1980. Microcrack closure in rocks under stress: direct observation. J. Geophys. Res., **85**, 7072-7090.

Birch, F., 1960. The velocity of compressional waves to 10 Kbar, Part I. J. Geophys. Res., **65**, 1083-1102.

Bonner, B.P., 1974. Shear wave birefringence in dilating granite. Geophys. Res. Let., **1**, 217-220.

Brace, W.F., B.W. Paulding, Jr. and C. Scholz, 1966. Dilatancy in the fracture of crystalline rocks, J. Geophys. Res., **71**, 3939-3953.

Brace, W.F., J.B. Walsh and W.T. Frangos, 1968. Permeability of granite under high pressure. J. Geophys. Res., **73**, 2225-2236.

Brace, W.F., E. Silver, K. Hadley and C. Goetze, 1972. Cracks and pores: A closer look. Sience, **178**, 162-164.

Cheng, C.H. and M.N. Toksöz, 1979. Inversion of seismic velocities for the pore aspect ratio spectrum of a rock. J. Geophys. Res., **84**, 7533-7543.

Clark, Jr., S.P., 1966. Handbook of physical constants. The geological society of America.

Eshelby, J.D., 1957. The determination of the elastic field of an ellipsoidal inclusion and related problems. Proc. Roy. Soc., Ser. A, **241**, 376-396.

Franklin, J.N., 1970. Well-posed stochastic extensions of ill-posed linear problems. J. Math. Anal. Appl., **31**, 628-716.

Fujii, N. and Y. Hamano, 1977. Anisotropic changes in resistivity and velocity during rock deformation, in High Pressure Research: Applications to geophysics. edited by M.H. Manghani and S. Akimoto, Academic Press, 53-63.

Garbin, H.D. and L. Knopoff, 1973. The compressional modulus of a material permeated by a random distribution of circular cracks. Q. Appl. Math., **30**, 453-464.

Gupta, I.N., 1973. Seismic velocities in rock subjected to axial loading up to shear fracture. J. Geophys. Res., **78**, 6936-6942.

Cadley, K., 1975. Azimuthal variation of dilatancy. J. Geophys. Res., **80**, 4845-4850.

Hadley, K., 1976. Comparison of calculated and observed crack densities and seismic velocities in Westerly granite. J. Geophys. Res., **81**, 3484-3494.

Ikeda, R. and H. Takahashi, 1981. Stress measurement by hydrofracturing at Futtsu city, Chiba prefecture. Zisin (J. Seis. Soc. Japan), **34**, 565-576 (in Japanese).

Jaegar, J.C. and N.G.W. Cook, 1971. Fundamentals of rock mechanics. Chapman and Hall.

Kranz, R.L., 1979. Crack-crack and crack-pore interactions in stressed granite. Int. J. Rock Mech. Min. Sci. & Geomech. Abstr., **16**, 37-47.

Kuster, G.T. and M.N. Toksöz, 1974. Velocity and attenuation of seismic waves in two-phase media, I, Theoretical formulations. Geophysics, **39**, 587-607.

Lockner, D.A., J.B. Walsh and J.D. Byerlee, 1977. Changes in seismic velocity and attenuation during deformation of granite. J. Geophys. Res., **82**, 5374-5378.

Love, A.E., 1934. A treatise on the mathematical theory of elasticity. Cambridge University Press.

Maeda, I., 1979. On the apparatus for fracture experiments using large size samples. Geophys. Bull. Hokkaido Univ., **38**, 55-61 (in Japanese).

Maeda, I. and N. Shimizu, 1983. A new method of measuring in-situ stress. J. Fac. Sci. Hokkaido Univ., Ser. 7 (Geophysics), **7**, 257-267.

Mavko, G.M. and A. Nur, 1978. The effect of nonelliptical cracks on the compressibility of rocks. J. Geophys. Res., **83**, 4459-4468.

Mogi, K., 1962. Study of elastic shocks caused by the fracture of heterogeneous materials and its relations to earthquake phenomena. Bull. Earthq. Res. Inst., Tokyo Univ., **40**, 125-173.

Mogi, K., 1968. Source locations of elastic shocks in the fracturing process in rocks (1). Bull. Earthq. Res. Inst., Tokyo Univ., **46**, 1103-1125.

Moss, W.C. and Y.M. Gupta, 1982. A constitutive model describing dilatancy and cracking in brittle rocks. J. Geophys. Res., **87**, 2985-2998.

Nishizawa, O., K. Kusunose and K. Onai, 1981. A study of space-time distribution of AE hypocenters in a rock sample under uniaxial compression. Bull. Geol. Surv. Japan, **32**, 473-486.

Nur, K. and J. Simmons, 1969a. Stress-induced velocity anisotropy in rock: an experimental

study. J. Geophys. Res., **74**, 6667-6674.
Nur, A. and G. Simmons, 1969b. The effect of saturation on velocity in low porosity rocks. Earth Planet. Sci. Let., **7**, 183-193.
Nur, A., 1971. Effects of stress on velocity anisotropy in rocks with cracks. J. Geophys. Res., **76**, 2022-2034.
O'Connell, R.J. and B. Budiansky, 1974. Seismic velocities in dry and saturated cracked solids. J. Geophys. Res., **79**, 5412-5426.
Olsson, W.A. and S.S. Peng, 1976. Microcrack nucleation in marble. Int. J Rock Mech. Min. Sci. & Geomech. Abstr., **13**, 53-59.
Sato, T., 1978. A note on body wave radiation from expanding tension crack. Sci. Rep. Tohoku Univ., Ser. 5 (Geophysics), **25**, 1-10.
Scholz, C.H., 1968 a. Experimental study of the fracturing process in brittle rock. J. Geophys. Res., **73**, 1447-1454.
Scholz, C.H., 1968b. Microfracturing and the inelastic deformation of rock in compression. J. Geophys. Res., **73**, 1417-1432.
Scholz, C.H. and T.A. Koczynski, 1979. Dilatancy anisotropy and the respose of rock to large cyclic loads. J. Geophys. Res., **84**, 5525-5534.
Shimizu, N. and I. Maeda, 1980. Anisotropic changes of compressional wave velocity and attenuation under uniaxial compression. Coll. Abstr. Autumn Meet, Seis. Soc. Japan, 143 (in Japanese).
Shimizu, N. and I. Maeda, 1982. The effect of velocity anisotropy on AE source locations in a very large granite sample. J. Fac. Sci. Hokkaido Univ., Ser. 7 (Geophysics), **7**, 135-144.
Simmons, G. and W.F. Brace, 1965. Comparison of static and dynamic measurements of compressibility of rocks. J. Geophys. Res., **70**, 5649-5656.
Simmons, G. and H. Wang, 1971. Single crystal elastic constants and calculated aggregate properties: A handbook. The M.I.T. Press.
Sneddon, I.N. and M. Lowengrub, 1969. Crack problems in the classical theory of elasticity. John Wiley & Sons.
Soga, N., H. Mizitani, H. Spetzler and R.J. Martin III, 1978. The effect of dilatancy on velocity anisotropy in Westerly granite. J. Geophys. Res., **83**, 4451-4458.
Sprunt, E.S. and W.F. Brace, 1974. Direct observation of microcavities in crystalline rocks. Int. J. Rock Mech. Min. Sci. & Geomech. Abstr., **11**, 139-150.
Stevens, J.L. and D.J. Holcomb, 1980. A theoretical investigation of the sliding crack model of dilatancy. J. Geophys. Res., **85**, 7091-7100.
Tapponnier, P. and W.F. Brace, 1974. A closer look at dilatant microcracks. Eos Trans. AGU, **56**, 1195.
Tapponnier, P. and W.F. Brace, 1976. Development of stress induced microcracks in Westerly granite. Int. J. Rock Mech. Min. Sci. & Geomech. Abstr., **13**, 103-112.
Tocher, D., 1957. Anisotropy in rocks under simple compression. Eos Trans. AGU, **38**, 89-94.
Toksöz, M.N., C.H. Cheng and A. Timur, 1976. Velocities of seismic waves in porous rocks. Geophysics, **41**, 621-645.
Walsh, J.B., 1965 a. The effect of cracks on the compressibility of rock. J. Geophys. Res., **70**, 381-389.
Walsh, J.B., 1965b. The effect of cracks on the uniaxial elastic compression of rocks. J. Geophys. Res., **70**, 399-411.
Walsh, J.B. and M.A. Grosenbaugh, 1979. A new model for analyzing the effect of fractures on compressibility. J. Geophys. Res., **84**, 3532-3536.
Wu, T.T., 1966. The effect of inclusion shape on the elastic moduli of a two-phase material. Int. J. Solids Struct., **2**, 1-8.

APPENDIX A

The tensors S_{ij} are given by the following expressions:

$$S_{11}(=S_{22})=S_{1111}=\frac{3}{4}(1-R)\left(1-\frac{1}{2}f\right)+\frac{1}{2}R\Phi,$$

$$S_{12}(=S_{21})=S_{1122}=\frac{1}{4}(1-R)\left(1-\frac{1}{2}f\right)-\frac{1}{2}R\Phi,$$

$$S_{13}(=S_{23})=S_{1133}=\frac{1}{2}(1-R)\alpha^2 f-\frac{1}{2}R\Phi,$$

$$S_{31}(=S_{32})=S_{3311}=\frac{1}{2}(1-R)f-R(1-\Phi),$$

$$S_{33}=S_{3333}=(1-R)(1-\alpha^2 f)+R(1-\Phi),$$

$$S_{44}(=S_{55})=S_{2323}=\frac{1}{4}(1-R)(1+\alpha^2)f+\frac{1}{4}R(2-\Phi),$$

$$S_{66}=S_{1212}=\frac{1}{4}(1-R)\left(1-\frac{1}{2}f\right)+\frac{1}{2}R\Phi,$$

where

$$\Phi=\frac{\alpha}{(1-\alpha^2)^{3/2}}\{\cos^{-1}\alpha-\alpha(1-\alpha^2)^{1/2}\},$$

$$f=\frac{2-3\Phi}{1-\alpha^2},$$

$$R=\frac{3G}{3K+4G}.$$

APPENDIX B

The two scalar functions T_K and T_G are given by the following expressions:

$$T_K=\frac{3F_1}{F_2}$$

$$T_G=\frac{2}{F_3}+\frac{1}{F_4}+\frac{F_4F_5+F_6F_7-F_8F_9}{F_2F_4}$$

where

$$F_1=1+A\left\{\frac{3}{2}(g+\Phi)-R\left(\frac{3}{2}g+\frac{5}{2}\Phi-\frac{4}{3}\right)\right\}$$

$$F_2=1+A\left\{1+\frac{3}{2}(g+\Phi)-\frac{R}{2}(3g+5\Phi)\right\}+B(3-4R)$$

$$+\frac{A}{2}(A+3B)(3-4R)\{g+\Phi-R(g-\Phi+2\Phi^2)\}$$

$$F_3=1+\frac{A}{2}\left\{R(2-\Phi)+\frac{1+\alpha^2}{\alpha^2}g(R-1)\right\}$$

$$F_4=1+\frac{A}{4}\{3\Phi+g-R(g-\Phi)\}$$

$$F_5=A\left\{R\left(g+\Phi-\frac{4}{3}\right)-g\right\}+B\Phi(3-4R)$$

$$F_6=1+A\{1+g-R(g+\Phi)\}+B(1-\Phi)(3-4R)$$

$$F_7=2+\frac{A}{4}\{9\Phi+3g-R(5\Phi+3g)\}+B\Phi(3-4R)$$

$$F_8=A\left\{1-2R+\frac{g}{2}(R-1)+\frac{\Phi}{2}(5R-3)\right\}+B(1-\Phi)(3-4R)$$

$$F_9=A\{g(R-1)-R\Phi\}+B\Phi(3-4R)$$

$$A=\frac{G'}{G}-1,\quad B=\frac{1}{3}\left(\frac{K'}{K}-\frac{G'}{G}\right),\quad R=\frac{3G}{3K+4G}$$

$$\Phi=\frac{\alpha}{(1-\alpha^2)^{3/2}}\{\cos^{-1}\alpha-\alpha(1-\alpha^2)^{\frac{1}{2}}\}$$

$$g=\frac{\alpha}{1-\alpha^2}(3\Phi-2).$$

APPENDIX C

The behavior of the closing of a penny-shaped crack under the application of compressive stress, where the direction is oblique to crack normals, is obtained by investigating the deformation of a crack in the limit of $\alpha\to 0$ in terms of equation (3.2.3). The relative volume change of a crack due to differential stress is given as

$$e_v^0=\lim_{\alpha\to 0} e_V=-\cos^2\theta\,\frac{4(1-\nu^2)P}{\pi\alpha E}.$$

When the differential stress P is applied to the crack with a unit volume initially, the condition of closing of this crack is

$$1+e_V^0=0.$$

In other words, the differential stress required for the closing of a crack is

$$P'=\frac{\pi\alpha E}{4(1-\nu^2)\cos^2\theta}.$$

When $\theta=0^\circ$, this expression is equivalent to the result obtained by Walsh (1965a) and we will denote this closing stress by P_{close}. If we represent the deformation of a penny-shaped crack in terms of the normalized differential stress, namely, $a=P/P_{close'}$ we obtain the following expression for the relative volume change of a penny-shaped crack due to differential stress, $f(a)$,

$$f(a)=1-a\cdot\cos^2\theta=1-\frac{a}{2}-\frac{a}{2}\cos 2\theta.$$

APPENDIX D

The explicit expressions for $\tilde{C}_{ijkl}$ are obtained by using the following equation,

$$\tilde{C}_{ijkl}=C_{ijpq}A_{pqkl}$$

where C_{ijkl} is the crack-free elastic constants and A_{pqkl} is defined in equation (3.2.6). The explicit forms for each $\tilde{C}_{ijkl}$ are given neglecting the second and higher order terms in the limit of $a\to 0$ as follows:

$$\tilde{C}_{1111}=\tilde{C}_{2222}=\tilde{C}_{1122}=\tilde{C}_{2211}=\left(K+\frac{4}{3}G\right)\frac{(1-2R)^2}{\pi aR(1-R)},$$

$$\tilde{C}_{3333}=\left(K+\frac{4}{3}G\right)\frac{1}{\pi aR(1-R)},$$

$$\tilde{C}_{2233}=\tilde{C}_{3322}=\tilde{C}_{3311}=\tilde{C}_{1133}=\left(K+\frac{4}{3}G\right)\frac{1-2R}{\pi aR(1-R)},$$

$$\tilde{C}_{2323}=\tilde{C}_{2332}=\tilde{C}_{3232}=\tilde{C}_{3223}=\tilde{C}_{3131}=\tilde{C}_{3113}=\tilde{C}_{1313}=\tilde{C}_{1331}$$
$$=\left(K+\frac{4}{3}G\right)\frac{4R}{\pi a(3-2R)}$$

$$\tilde{C}_{1212}=\tilde{C}_{1221}=\tilde{C}_{2121}=\tilde{C}_{2112}=\left(K+\frac{4}{3}G\right)R,$$

otherwise is zero,

where

$$R=\frac{3G}{3K+4K}.$$

Here $\tilde{C}_{1212}$ is a quantity much less than other quantities. If we consider that $\tilde{C}_{1212}$ is the quantity of order (0), a condition where these quantities are the axial symmetry with respect to the load axis, namely,

$\frac{\tilde{C}_{1111}-\tilde{C}_{1122}}{2}=\tilde{C}_{1212}$, is satisfied.